People's Democratic Republic of Algeria

Ministry of Higher Education and Scientific Research

University M'Hamed BOUGARA - Boumerdes

Institute of Electrical and Electronic Engineering
Department of Power and Control

Final Year Project Report Presented in Partial Fulfillment
of the Requirements for the Degree of

MASTER

In **Control Engineering**

Title:

Control of Three-Phase Inverter Grid-connected Solar system

Presented by :

Soumeya HAMBLI

Supervisor :

Dr. Brahim METIDJI

Registration Number ..... /2024

Abstract

Grid-connected solar photovoltaic (PV) systems are rapidly increasing each year due to a growing global interest in renewable energy and rising energy demand. This project focuses on designing and modeling a grid-connected PV system using space vector pulse width modulation (SVPWM). It also reviews key aspects and literature related to the components of a PV system, the inverter, and the grid connection. The photovoltaic model is employed to replicate the characteristics of a real PV array, while a Perturb and Observe method for maximum power point tracking (MPPT) is introduced to optimize the DC-DC boost converter's performance. In this project, a three-phase two-level voltage source inverter (VSI) is employed, controlled using two approaches: a synchronous reference frame with a proportional-integral (PI) controller and a stationary reference frame with a proportional-resonant (PR) controller with space vector pulse width modulation (SVPWM). The control strategy includes a phase-locked loop (PLL) to acquire important data about the grid voltage. To connect the inverter output to the grid, an LCL filter is used to reduce total harmonic distortion (THD) in both the output current and voltage. The system model is created using the MATLAB/SIMULINK environment.

Dedication

I dedicate this modest work to my beloved parents, thank you for your endless love and support; you are my safe haven. I am forever grateful for everything you have done for me, my sister and brother, my sister from another mother, *Kahina*, my lovely *Kami*, my special friends *Sarra, Maria, Selma, Rayane* and all those I love.

Acknowledgment

In the name of Allah the Most Beneficent and the Most Merciful, we thank Allah for all His blessing and strength that He gives us in completing this modest project.

I would like to express my sincere gratitude to our supervisor, Dr.BRAHIM METIDJI,

Thank you for your guidance and assistance during the realization of this work.

I especially thank Rayane GHERAOUT, Amina HAMBLI and Yacine BELKADI for their help and guidance throughout my work.

I would like to extend my thanks to everyone who has been

a support, to all my friends, and my great teachers.

Soumeya HAMBLI

List of Figures

List of Tables

DC/AC	Direct Current /Alternating Current
DC/DC	Direct Current /Direct Current
PWM	Pulse Width Modulation
PV	Photovoltaic
MPPT	Maximum Power Point Tracking
AC	Alternating Current
DC	Direct Current
PI	Proportional Integral
PR	Proportional Resonant
P&O	Perturb and Observe
MPP	Maximum Power Point
CSI	Current Source Inverter
VSI	Voltage Source Inverter
PLL	Phase Locked Loop
SVPWM	Space Vector Pulse Width Modulation
SPWM	Sinusoidal Pulse Width Modulation
RAF	Ripple Attenuation Factor
SVM	Space Vector Modulation
SRF	Synchronous Reference Frame
PSO	Particle Swarm Optimization
SRRF	Synchronously rotating reference frame
THD	Total Harmonic Distortion
C	Capacitor
R	Resistor
L	Inductor
d-q	Direct-quadrature
α-β	Alpha Beta
Kp	Proportional gain
Ki	Integral gain
Kr	Resonant gain

General Introduction

In the past decade, attention has increasingly shifted towards renewable energy sources instead of fossil fuels. This change has initiated extensive research in wind and solar energy, which provide abundant, clean, and sustainable energy with minimal environmental impact.

A Solar Photovoltaic (PV) system employs solar cells to convert solar energy into electrical power. A solar cell, also known as a PV cell, is an electrical device that produces electricity directly from sunlight.

Utilizing renewable energy sources has become a crucial and promising way to obtain new energy to satisfy the growing global demand for power. Total harmonic distortion, which reduces power quality, is a critical concern in grid-connected solar power systems.

A grid-connected solar PV system is unlike traditional power distribution systems. Managing the flow of active and reactive power can be quite difficult, and different strategies are needed to ensure the system operates synchronously again.

This project aims to improve the performance and stability of a three-phase inverter linked to the electrical grid by employing two distinct transformation techniques: stationary reference frame and synchronous Reference Frame. These approaches manipulate the voltage and current of the grid, which are crucial for enhancing the system's efficiency, reliability, stability, and power quality through independent control of active and reactive power. When the active power achieves an optimal level, it can be supplied to the grid via the inverter, while the reactive power can be modified to the required level.

This project begins with Chapter 1, which delivers a thorough theoretical overview. It begins with an introduction to photovoltaic cells and their operation and addresses essential topics such as maximum Power Point tracking (MPPT) techniques, DC-DC boost converters, and the functioning of DC-AC inverters.

Chapter 2 shifts to system modeling and control strategies for photovoltaic inverter applications. It investigates the grid-connected inverter system's modeling and the characteristics of photovoltaic cells and modules. The chapter delves into DC-DC converter design, emphasizing the Perturb and Observe MPPT algorithm, and analyzes control structures for grid-connected inverters, including advanced techniques for representing three-phase variables. The chapter also highlights Space Vector Pulse Width Modulation (SVPWM)

strategies, and the comprehensive system block diagram lays a strong groundwork for effective inverter control.

Finally, Chapter 3 focuses on simulation and results analysis, shedding light on the operational characteristics of both DC-DC and DC-AC converters. It examines the DC-Link voltage and presents voltage and current waveforms under various control strategies, particularly comparing Proportional-Integral (PI) and Proportional-Resonant (PR) controllers.

Chapter 1
Theoretical Background

1.1 Introduction

This chapter provides a foundational overview of photovoltaic (PV) systems. It covers the basics of photovoltaic cells and their types, various PV system configurations, and critical technologies for performance optimization. Key topics include Maximum Power Point Tracking (MPPT), DC-DC boost converters, and DC-AC inverters. The chapter also addresses the management of active and reactive power, grid synchronization, power decoupling, modulation techniques, and the role of filters as grid interfaces. This introduction sets the stage for a deeper analysis in subsequent chapters.

1.2 Overview of Photovoltaic Cell

A photovoltaic cell, commonly called a solar cell, converts sunlight directly into electrical energy without requiring any rotating parts. These cells are fundamental components of solar PV systems. Composed of semiconductors, photovoltaic cells function much like other solid-state electronic devices such as diodes, transistors, and integrated circuits. For practical applications, these cells are typically organized into modules and arrays [1].

Types of PV Cells

There are various types of photovoltaic cells available on the market, and different other types of cells are under development [2].

Monocrystalline Solar Cell

These photovoltaic cells, known as "single crystalline" cells, are easily identifiable by their color. They are considered distinct because they are made from a very pure type of silicon. In the silicon industry, the efficiency of a material depends on the purity and alignment of its molecules, with these cells achieving an efficiency of around 20%. Solar cells convert sunlight into electricity and are constructed from "silicon ingots," which are cylindrical to improve performance. Consequently, panels with mono-crystalline cells have rounded edges rather than the square shapes typical of other solar cells. This design requires fewer cells per unit of electrical output. Additionally, these cells boast the greatest longevity among solar cell types.

Polycrystalline Solar Cell

Unlike mono-crystalline cells, these cells do not need to be cut. Instead, the silicon is placed into square molds, creating square-shaped cells. This approach is more cost-effective because it minimizes silicon waste during manufacturing. Typically, the efficiency of these cells ranges from 13-16%, primarily due to the lower purity of the silicon used.

Amorphous Solar Cell

This type of cell is composed of thin films made from amorphous silicon, typically used for low-power applications. A recent advancement called "stacking" involves layering multiple amorphous silicon cells to achieve higher efficiency, reaching up to 8%. Despite this increase in efficiency, the technique is quite costly.

1.3 Types of solar PV system

From application perspective, photovoltaic power systems are categorized into two types: grid-connected and off-grid. They can be designed to produce either DC or AC voltage and can operate either independently of the grid or in conjunction with it [3].

1.3.1 Grid connected PV system

In grid-connected PV systems, the inverter, or power conditioning unit (PCU), is the essential component. The PV system produces a small amount of DC power, which must be converted to AC power suitable for the grid through the inverter. Therefore, the PV inverter is crucial in a grid-connected PV system. In such a system, any excess power is fed into the grid. Moreover, when sunlight is insufficient or absent, power is drawn from the grid, thereby eliminating the need for a battery. The DC power generated by the PV system is first converted to AC power by the inverter, harmonics are filtered, and the voltage level is adjusted before the AC power is fed into the grid. Figure 1.1 describes the block diagram of a grid connected PV system.

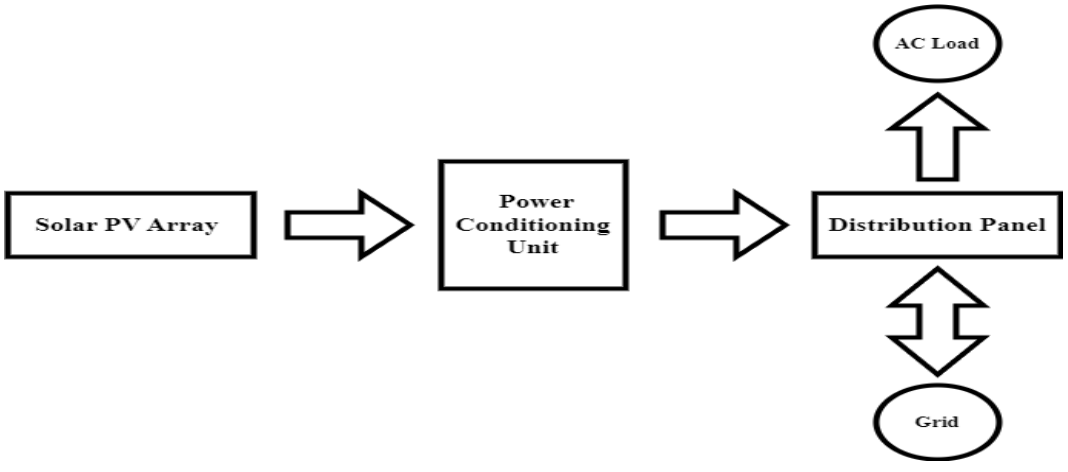

Figure 1.1: Block diagram of grid connected solar PV system

1.3.2 Stand-Alone Photovoltaic Systems

An off-grid solar PV system operates independently of the power grid. These systems are typically installed in remote locations, such as offshore islands or rural areas where the power grid is not accessible. They can also be used in cities where connecting to the power grid is either impractical or too costly. Off-grid systems utilize deep cycle rechargeable batteries, including nickel-cadmium, lead-acid, or lithium-ion, to store electricity for times when the solar PV system generates little or no power, such as during nighttime. Stand-alone PV systems are typically used for low-power needs, providing specific DC and/or AC electrical loads. To ensure the load operates both during daylight and nighttime hours using PV power, energy storage devices (batteries) are required, making the system more expensive. Figure 1.2 shows the block diagram of a standalone PV system where the PV array is connected to DC and AC loads through a charge controller.

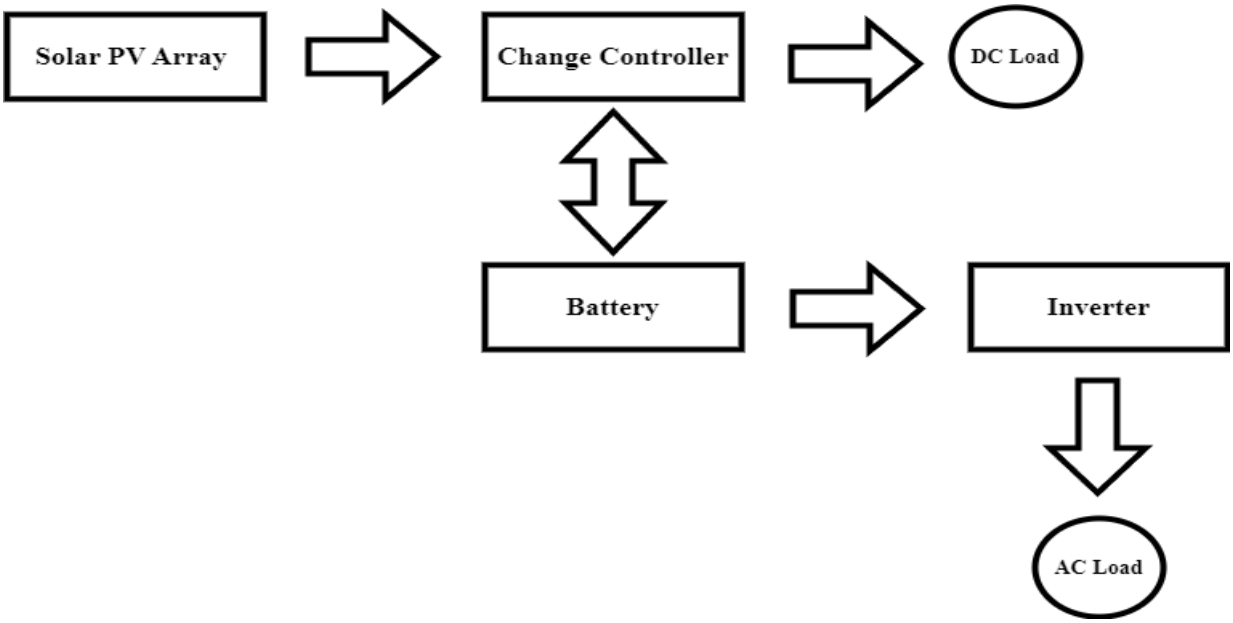

Figure 1.2: Block diagram of standalone PV system with battery storage

1.4 Maximum Power Point Tracking

The maximum power point tracking is the main part of the solar PV system. It is essential for extracting the maximum power from the PV array. The output power of the PV array is influenced by factors such as solar irradiance and temperature. Below is a summary of the most commonly utilized MPPT algorithms.

1.4.1 Perturb and Observe Algorithm

This algorithm operates by perturbing a control variable, which can be either the output voltage of the PV array or the duty cycle of the DC-DC converter switches. In the first method, a perturbation is applied to the PV array's output voltage, and a PI controller adjusts the converter's duty ratio based on this. The PI controller is calibrated using the maximum power point of the PV array's voltage [4]. In the direct duty cycle control method, a small perturbation is directly introduced into the duty cycle of the DC-DC converter. A major advantage of Perturb and Observe algorithm is that it is simple and easy to implement. Figure 1.3 shows the flowchart for the direct duty ratio control P&O algorithm.

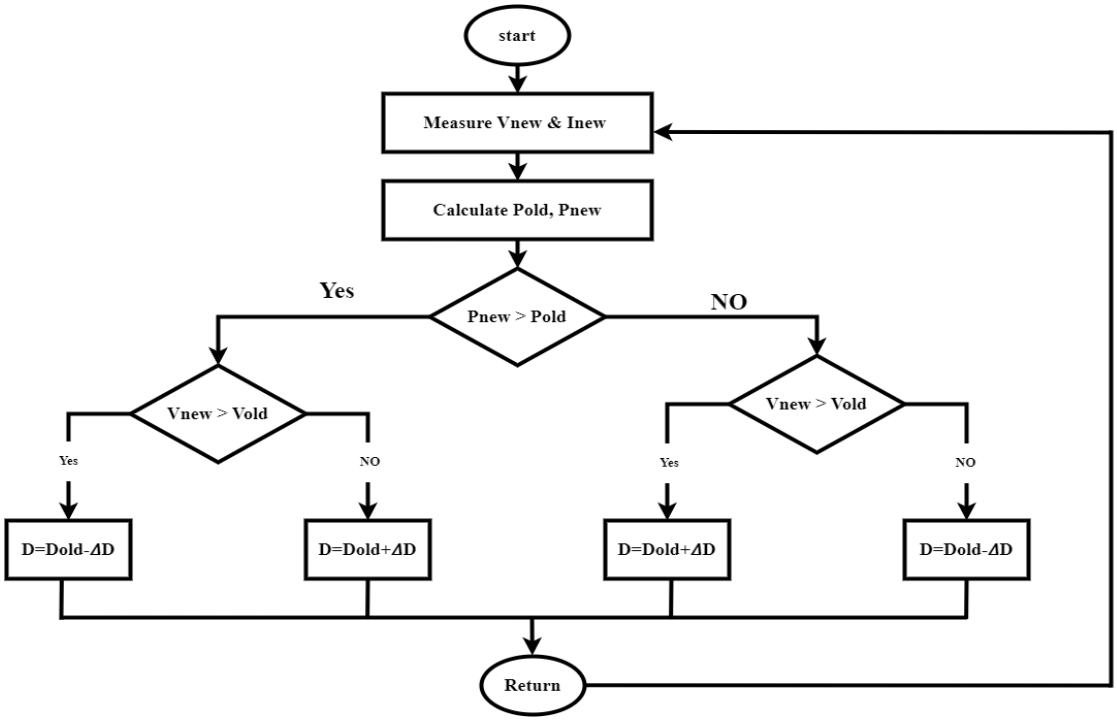

Figure 1.3: Flowchart of perturb and observe algorithm

Figure 1.4 shows the Perturb and Observe method for MPPT

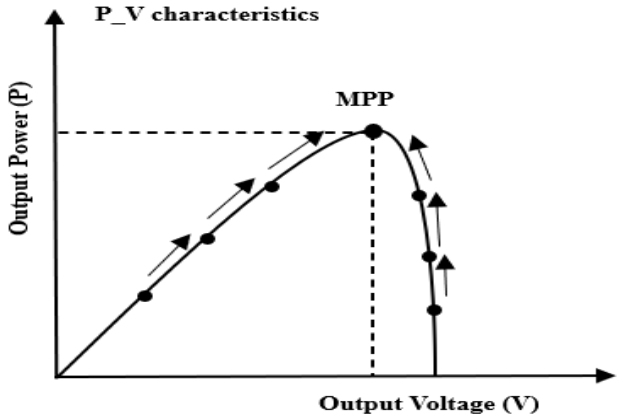

Figure 1.4: Perturb and observe method for MPPT

1.4.2 Incremental Conductance Algorithm

In this algorithm, the power of the PV array, which is the product of voltage and current, is differentiated with respect to the PV array voltage and set to zero. The actual operating point is then determined based on this differential value. Unlike the perturb and observe method, this approach does not require the direct calculation of PV array power. It provides excellent transient performance, particularly in varying atmospheric conditions. Figure 1.5 presents the flowchart for the Incremental Conductance algorithm.

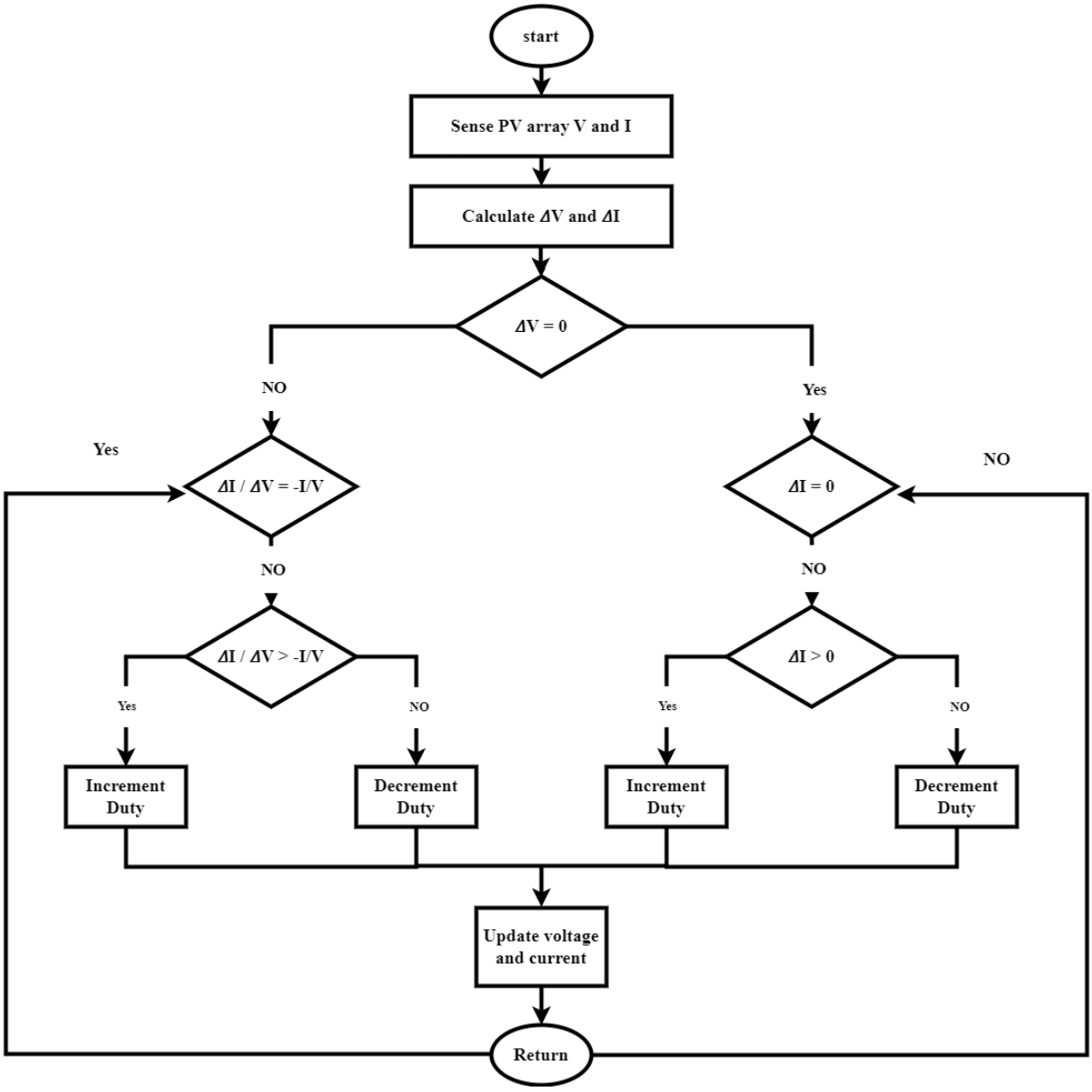

Figure 1.5: Flowchart of incremental conductance algorithm

The core concept of the incremental conductance method is that the slope of the power with respect to the voltage is zero at the Maximum Power Point (MPP). Power increases as voltage rises to the left of the MPP and decreases as voltage rises to the right. In other words,

the slope of the PV curve is zero at the MPP, positive to the left of it, and negative to the right [5]. Figure 1.6 shows the incremental conductance method for MPPT.

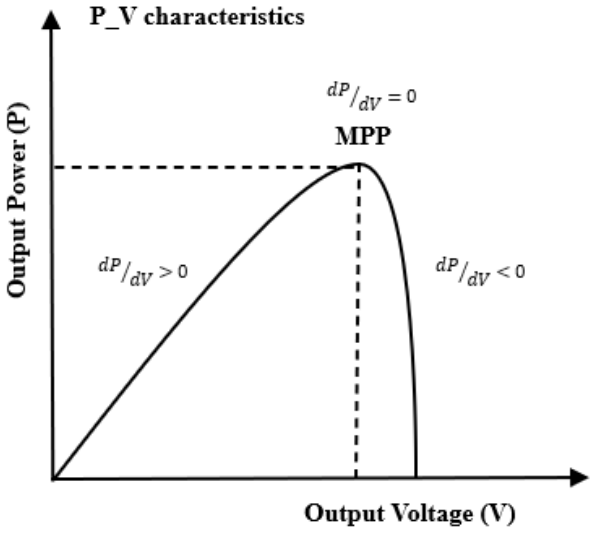

Figure 1.6: Incremental conductance method for MPPT

1.5 DC-DC Boost converter

The Boost converter is a type of power converter that produces an output voltage higher than its input voltage. It comprises four primary components: an inductor, a power electronic switch (like an IGBT or MOSFET), a diode, and a capacitor. The operation of the boost converter is controlled by Pulse Width Modulation (PWM), which regulates the device by frequently switching the power switch *ON* and *OFF* at a specific frequency, known as the switching frequency [6],[7].

1.6 DC-AC Inverter in PV System

Modern inverters used in PV systems are self-commutated. The switching devices employed can be power BJTs, IGBTs, or MOSFETs, depending on the system's switching frequency and power density. They are generally classified into two main types: current source inverters and voltage source inverters. A brief overview of these types is provided below [8].

1.6.1 Current Source Inverter

In a current source inverter (CSI), the input is a current source with a fixed polarity, and the power flow direction is controlled by the input voltage. The CSI generates an alternating current wave at the output, which maintains a constant magnitude based on the

input but allows for adjustments in the time period. To maintain stable current, an inductor is connected to the input side of the CSI.

1.6.2 Voltage Source Inverter

In a voltage source inverter (VSI), the input is a voltage source, typically provided by a large capacitor. The input voltage's polarity remains constant, so the direction of power flow is regulated by the DC current input. Unlike current source inverters (CSIs), VSIs can produce an alternating voltage with a fixed amplitude but a variable frequency. They also offer the flexibility to operate in either voltage control mode or current control mode.

1.7 Active and Reactive Powers and DC-Link Voltage Controller

The controller's functions are primarily managed through two cascaded loops [9]:

1. A rapid internal current loop that regulates the grid current to maintain high-quality power with low harmonic distortion.
2. An external voltage loop that manages the DC-link voltage to regulate the power flow within the system.

Clarke's Transformation

The conversion of a stationary circuit to a stationary reference frame was created by E. Clarke. In this transformation, the stationary two-phase variables are indicated as α and β [10]. As shown in figure below, α-axis and β-axis are orthogonal.

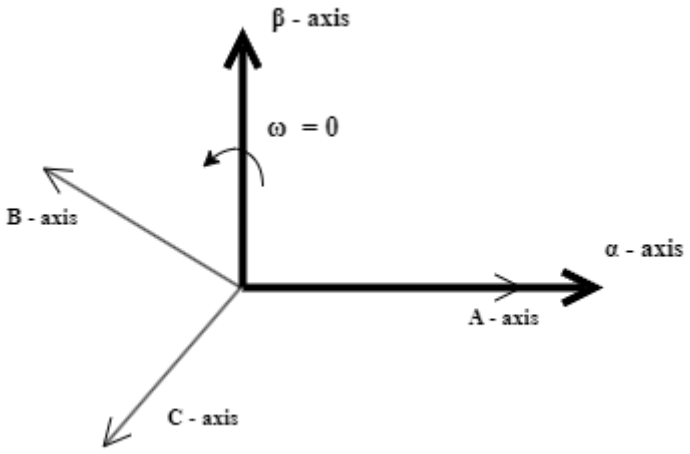

Figure 1.7: Clarke's Transformation

Park's Transformation

It is utilized to convert three-phase quantities into two-phase quantities within certain systems for control purposes. These variable transformations are employed in analyzing

various static and constant parameters in power system components. The transformation to an arbitrary reference frame encompasses all recognized real transformations for these components. This approach is a widely accepted method for three-phase to two-phase conversion in synchronous system analysis [10]. It is presented in the figure below.

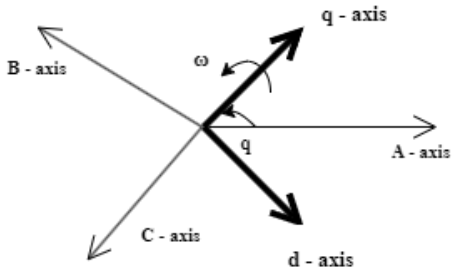

Figure 1.8: Park's Transformation

1.8 Grid synchronization

To achieve effective power flow between a renewable energy generator and the utility grid, the inverter current must be synchronized with the grid voltage. This process employs various algorithms aimed at accurately determining the phase information of the grid voltage. These algorithms may require transforming the reference frame from a natural to a stationary or synchronous frame to facilitate synchronization [9].

The zero-crossing method, along with grid voltage filtering and Phase-Locked Loop (PLL), are techniques employed for synchronizing with the grid. Of these three methods, PLL is the most commonly utilized. A brief overview of PLL is provided below.

Phase Locked Loop (PLL)

PLLs offer effective suppression of harmonics and other disturbances. They are implemented within a synchronous reference frame [11]. The basic structure of a PLL is depicted in Figure (1.8). To achieve phase locking, the reference d-axis voltage U_d^* is set to zero. A PI regulator is generally used to manage U_d, and the output of this regulator corresponds to the grid frequency, which can be integrated to determine the phase angle of the grid voltage.

- **Phase Detector**: The phase detector produces a signal proportional to the phase difference between the reference signal and the signal generated by the transformation block $(abc \rightarrow dq)$.

- **Loop Filter**: This part functions as a low-pass filter, often a PI controller, to filter out high-frequency AC components from the output of the phase detector. The output of this block represents the grid frequency.
- **VCO Controller**: This block integrates the grid frequency to determine the phase shift of the grid voltage (θ).

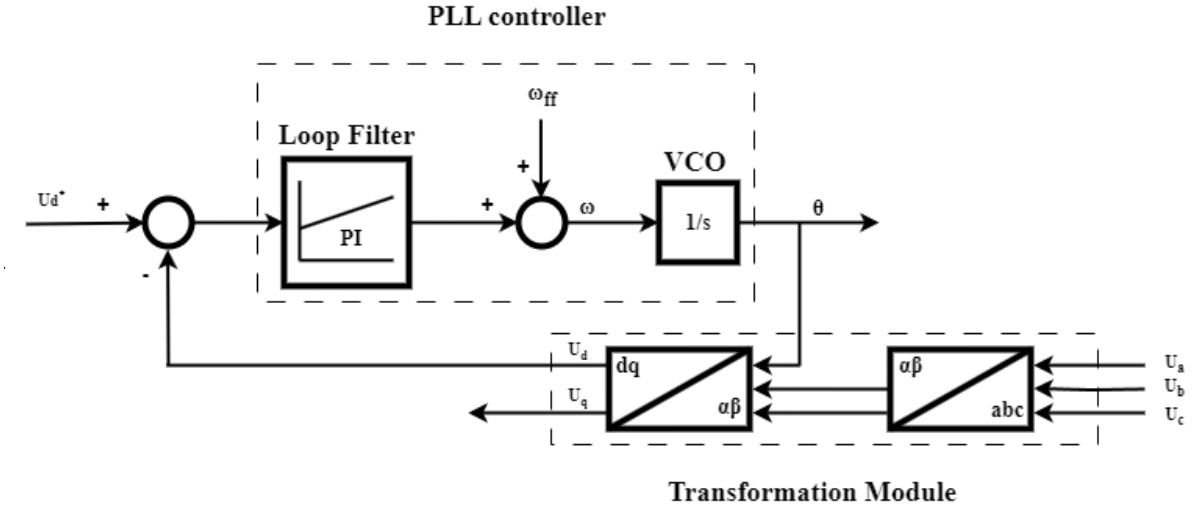

Figure 1.9: PLL loop

1.9 Power Decoupling

Power decoupling in a PV system is generally achieved with a capacitor. In a single-stage system, this capacitor is situated between the inverter and the PV panels. In a multistage system, it is located between the DC-DC converter's output and the inverter input. The purpose of the decoupling capacitor is to reduce the oscillations in the power generated by the PV modules [12].

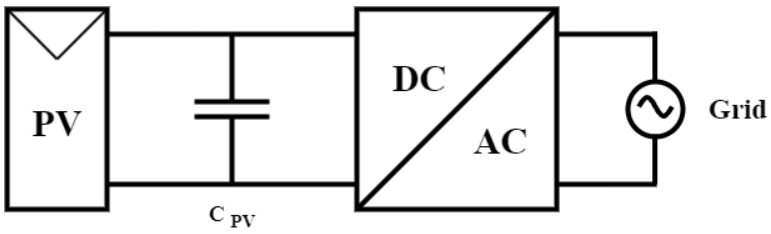

Figure 1.10: Capacitor location in multistage system

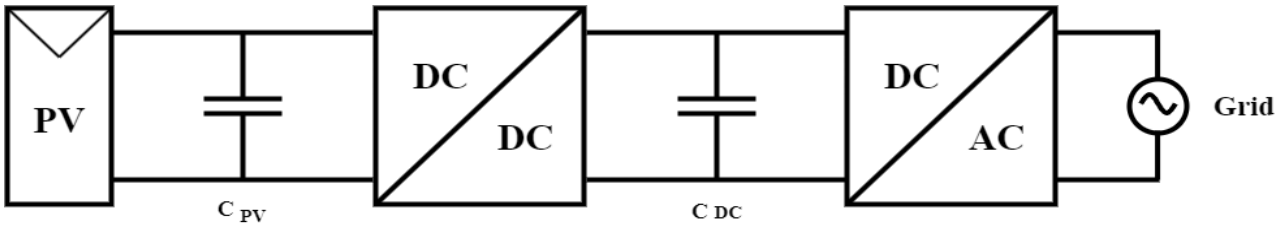

Figure 1.11: Capacitor location in multistage system

1.10 Modulation Techniques for Inverter

To convert DC voltage into an AC voltage signal, the inverter's switches must be toggled on and off by applying pulses to their gates. Various techniques can generate these pulses, with the most common being space vector pulse width modulation (SVPWM) and sinusoidal pulse width modulation (SPWM) [9]. This thesis will focus on SVPWM due to its simplicity in digital implementation and its capability to make full use of the DC bus voltage.

1.11 Filter as Grid Interface

Inverters, as switching devices, cannot be directly connected to the grid due to the harmonics they produce, which degrade power quality. Various standards limit the amount of harmonics that can be injected into the grid [13],[15]. One method to connect the system to the grid is by using a transformer, as the windings provide inductance that reduces the harmonics in the current wave [16]. However, transformers are expensive and bulky, making the system more costly. Consequently, a transformer-less approach has emerged, using a filter circuit as the interface. Three common types of passive filters are used: L, LC, and LCL filters, as illustrated in Figure 1.12.

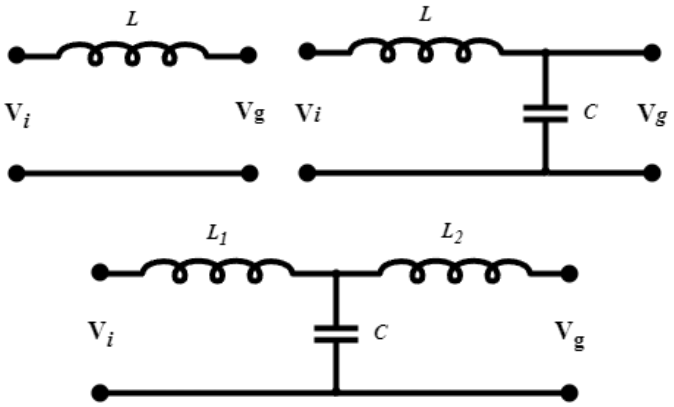

Figure 1.12: L, LC and LCL filters

1.12 Conclusion

This chapter outlined the essential elements of a grid-connected solar PV system, starting with an overview of photovoltaic cells and their types, followed by different solar PV systems. It included discussions on MPPT, DC-DC boost converters, and DC-AC inverters, alongside the management of active/reactive power, DC-link voltage, and grid synchronization. The chapter also covered power decoupling, modulation techniques for inverters, and the significance of filters as a grid interface, providing a solid base for the sections to come.

Chapter 2

System Modeling and Control Strategies of Photovoltaic Inverter

2.1 Introduction

This chapter presents the essential components and control techniques of a grid-connected photovoltaic system. It begins by reviewing photovoltaic cells and PV module modeling, then covers the design of a DC-DC boost converter and the Perturb & Observe MPPT algorithm to maximize energy output. Next, the chapter addresses the DC-AC inverter, the LCL filter for harmonic reduction, and the introduction of the Space Vector PWM method for effective inverter control. The second section centers on the inverter's control structure, examining the representation of three-phase variables, grid synchronization, and control loops for reliable performance, concluding with a system block diagram.

2.2 System Modeling of Photovoltaic Inverter

2.2.1 Overview of the Grid-Connected Inverter System

The grid-connected inverter system plays a pivotal role in integrating renewable energy sources, such as solar power, into the electrical grid. At the center of this system is the inverter, which is responsible for converting the direct current (DC) generated by solar panels into alternating current (AC) that aligns with the grid's requirements. The inverter not only ensures the proper synchronization of voltage, frequency, and phase with the grid but also manages the power flow between the solar array and the grid [17]. To enhance the quality of power fed into the grid, an LCL filter is utilized to attenuate harmonics and reduce electromagnetic interference, thereby ensuring the system operates smoothly and efficiently [18]. Furthermore, a boost converter is commonly utilized to increase the DC voltage from the solar panels to the necessary level for the inverter, maximizing energy transfer and enhancing the system's overall efficiency [19]. Collectively, these components constitute a unified system that facilitates the smooth integration of solar power into the grid, while ensuring both stability and efficiency. The ideal circuit model of a photovoltaic (PV) cell consists of an ideal current source connected in parallel with an ideal diode.

2.2.2 Photovoltaic Cell

The Photovoltaic (PV) cell is a P-N junction device constructed from semiconductor materials, typically composed of doped silicon [20]. The process of energy conversion in a PV cell can be outlined in three steps. Initially, the absorption of solar photons produces electron-hole pairs. Following this, the device's structure separates these electrons and holes. Lastly, the electric charges are collected at the PV cell's terminal. The rate of generation of electric charge depends on the solar irradiance, the temperature of the cell and the

semiconductor material type. The output power from a single PV cell is very low. A large number of PV cells are connected in series and parallel, making a PV module, to produce higher power levels [21]. Afterward, several modules are connected in series and parallel to create a PV array, as shown in the Figure 2.1.

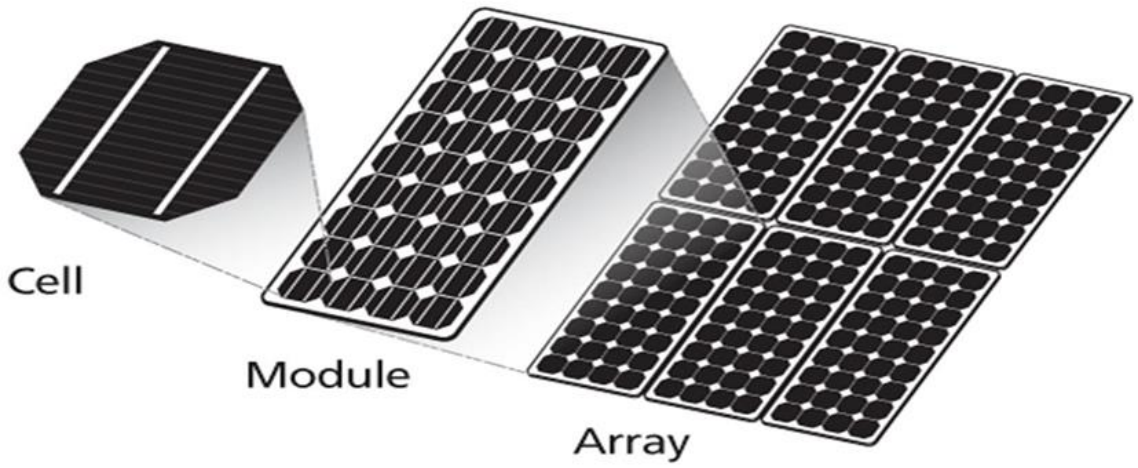

Figure 2.1: PV cell, module and array [21]

2.2.3 Modelling of PV Modules

A photovoltaic (PV) cell serves as the fundamental component and primary source within the power conversion system. It functions by converting light energy into electrical energy. To achieve higher voltage, PV cells are connected in series, while connecting them in parallel increases the current. The fundamental operation of the PV cell is based on the principles of a basic P-N junction semiconductor. The ideal circuit model of a PV cell consists of an ideal current source connected in parallel with an ideal diode. In this model, the diode defines the I-V characteristics of the solar cell, as illustrated in Figure 2.2. The term I_{ph} represents the photocurrent generated by the PV cell, which is influenced by solar irradiance and ambient temperature, while I_D refers to the shunt current flowing through the diode.

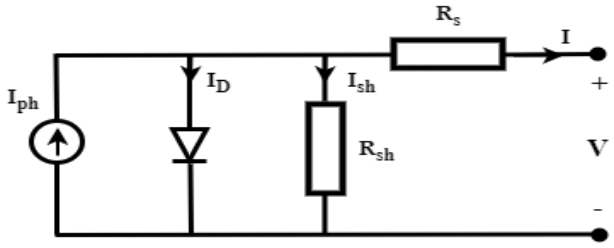

Figure 2.2: The equivalent circuit of PV cell

According to Kirchhoff's current law, the output current is given by [22]:

$$I = I_{ph} - I_D - \frac{V}{R_{sh}} \qquad (2.1)$$

Where I_{ph} is the photon current andI_j is the diode current and D is the parallel diode. R_{sh} is the shunt resistance and R_s is the series resistance. The current-voltage relationship of the PV cell is given by the (2.2) equation:

$$I = I_{ph} - I_0 \left\{ e^{\left(\frac{q.v}{AKT}\right)} - 1 \right\} - I_{sh} \qquad (2.2)$$

Where I_0 is the reverse saturation current of the diode.I_{ph} is the shunt current, q is the electron charge $q = 1.6 * 10 - 19\,C$, A is the current fitting factor, K is Boltzmann's constant $A = 1.381 * 10 - 23\,J\,/\,K$and T is the junction temperature (K). The resistance R_s is usually very low, while R_{sh} is considerably high. For simplification, R_s can be ignored in equation (2.2), leading to the equation:

$$I = I_{sh} - I_0 \left\{ e^{\left(\frac{q.v}{AKT}\right)} - 1 \right\} \qquad (2.3)$$

Where $I_{ph}$is the photon current and I_0 is the reverse saturation current of the diode.

In normal operating conditions, the standard test condition for irradiance is $1000\,[W/m^2]$and for the temperature is $T = 25^o[C]$. Figure 2.3 present the I-V and P-V characteristics of the PV panels, respectively. The current is shown to be directly proportional to the solar irradiance in this figure. Furthermore, the I-V and P_V characteristics of the PV panels exhibit non-linear relationships. Therefore, an MPPT algorithm is essential. Due to its simplicity, the MPPT technique most widely used is the perturb and observe (P&O) method [23]. The output voltage is the reference DC, either to the DC-AC inverter in the single-stage method or to the DC-DC inverter in the dual-stage method.

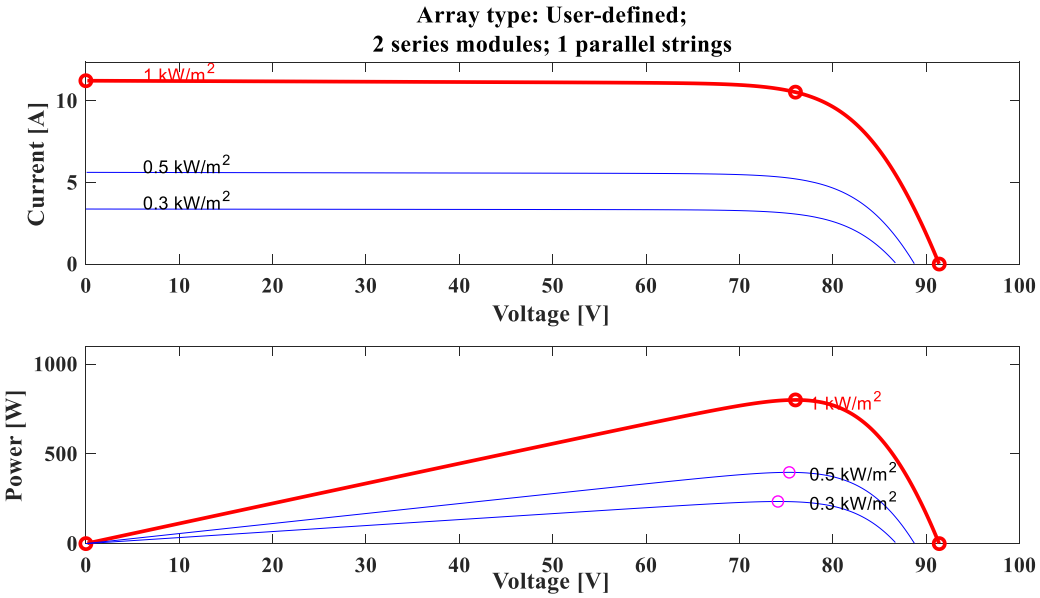

Figure 2.3: I-V and P-V characteristics of the PV panels

Table 2.1: Parameters for PV array

Parameter name	Specification values
Rated power	800 [W]
Open-circuit voltage (V_{oc})	45.7 [V]
Short-circuit current (I_{sc})	11.23 [A]
Temperature coefficient of I_{sc} (K_i) at $25^o[C]$ and 1000 $[W/m^2]$	0.102
Number of PV moduls connected in series	2
Number of PV moduls connected in parallel	1
Peak Voltage (V_{PV})	76 [V]
Peak Current (I_{PV})	10.53 [A]
Operating temperature (T)	25^O [C]
Solar irradiation(G)	1000 $[W/m^2]$

2.2.4 Modeling of Boost converter

In PV systems, DC/DC power converters are used to regulate the output voltage. Typically, a DC/DC converter is placed between the load and the PV panel to optimize the power drawn from the solar panel. This is particularly beneficial for PV systems with

unstable and varying output. When a PV system incorporates both AC and DC converters, a DC-link capacitor can improve the stability of the DC output voltage, thereby minimizing the impact of fluctuations on the AC output [24]. DC converters can operate as boost converters (increasing voltage), buck converters (decreasing voltage), or a combination of both, like CUK converters and buck-boost converters. The type of converter is chosen based on the required output voltage level, enabling the converter to provide the appropriate input voltage for the inverter while maintaining DC voltage stability and regulation [25]. This is crucial for hybrid energy systems, grid-connected systems, and standalone systems. In these configurations, the DC/DC converter operates with a maximum power point tracking algorithm to enhance the power output from the PV system. The basic circuit diagram of the boost converter employed in this study is shown in Figure 2.4.

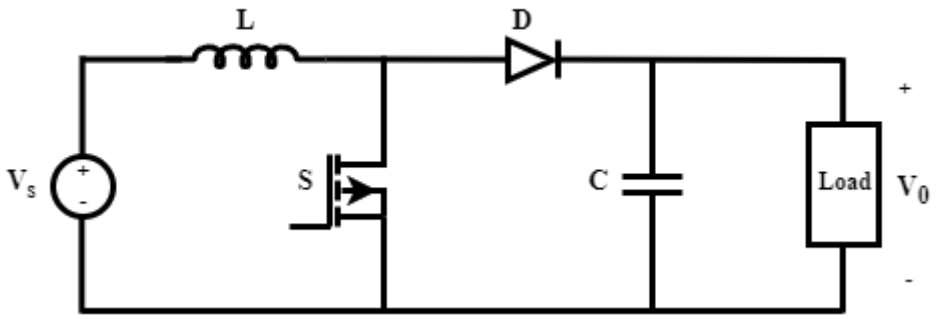

Figure 2.4: Circuit diagram of boost converter.

2.2.4.1 Design of DC-DC converter

Two stage topology is chosen for grid connected solar PV system. In this model, the DC-DC converter is used to raise the output voltage of the PV array to the required level, which is then fed into the inverter as input from the converter side. The switching device is a critical component in DC/DC conversion, chosen based on the system's design requirements, such as switching speed and power capacity. MOSFETs are generally selected for lower power capacity with high switching speed, while IGBTs are preferred for higher power capacity with moderate switching speed [26].

The boost converter receives an input voltage of $76V$ from the PV array, with the goal of achieving an output voltage of 200 [V]. The switching frequency for the IGBT switch is set at 5 [Khz].

The duty cycle of the boost converter is calculated using the formula (2.4) [26]

$$D = 1 - \frac{V_{PV}}{V_{DC-link}} \tag{2.4}$$

The boost inductor can be calculated using the formula (2.5) [26]

$$L > \frac{D(1-D)^2 R}{2f_s} \tag{2.5}$$

Where, V_{PV} is the input voltage to the converter, $V_{PV} = 76\ [V]$, V_0 is the desired output voltage, $V_0 = 200\ [V]$, f_s is the switching frequency in the boost converter which is chosen to be 5 [Khz].

The Photovoltaic capacitor can be calculated using the formula (2.6).

$$C_{PV} = \frac{V_{PV} D}{4\Delta V_{PV} f_s^2 L} \tag{2.6}$$

The DC-link capacitor can be obtained using the following formula (2.7).

$$C_{DC-link} = \frac{P_{PV}}{4\pi f_s V_0 \Delta V_0} \tag{2.7}$$

Where**,** P_{PV} the nominal power of PV module, f_s is the switching frequency, V_0 is the voltage across the capacitor, ΔV_0 is the amplitude of the ripple voltage which is chosen to be 3%.

Table 2-2: Design parameters for boost converter

Parameter name	**Value**
Output voltage of PV array at $1000\ [W/m^2]$ and $25^o[C]$	76 [V]
Output current of PV array at $1000\ [W/m^2]$and $25^o[C]$	10.53 [A]
Desired output voltage V_0	200 [V]
Output power of PV array at $1000\ [W/m^2]$and $25^o[C]$	800 [W]
Switching frequency f_{sw}	10000 [Khz]

The calculated values of each component used for this design are provided below.

Table 2.3: Boost converter calculated parameters

Parameter name	Value
Duty cycle (D)	62%
PV capacitor (C_{PV})	$1000e^{-6}$[F]
Inductance (L)	$1e^{-3}$[H]
DC-link capacitor ($C_{DC-Link}$)	$300e^{-6}$[F]
Resistance (R)	19 [Ω]

2.2.4.2 Perturb and Observe MPPT

The main purpose of the MPPT in a PV energy conversion system is to continuously optimize the system to extract the highest possible power from the solar array, regardless of varying weather or load conditions. Given that the solar array exhibits non-ideal voltage-current characteristics and factors like irradiance, ambient temperature, and wind which influence its output are unpredictable, the tracker must manage a nonlinear and time-varying system. Various algorithms can be employed to implement MPPT, including perturb & observe, incremental conductance, parasitic capacitance, and constant voltage. However, the most commonly used are the first two.

The Perturb and Observe (P&O) algorithm has been chosen as a MPPT control strategy in this thesis work. The P&O algorithm is a widely favored technique for MPPT in photovoltaic systems because of its simplicity and efficiency. The algorithm operates by making incremental changes to the system's voltage or current and observing the impact on power output. If the power output increases, the algorithm continues perturbing in the same direction; if the power output decreases, it reverses the direction of adjustment. This iterative approach aims to find and maintain the maximum power point of the solar array. However, the P&O algorithm can face challenges under rapidly fluctuating environmental conditions or during partial shading, where it may oscillate around the maximum power point rather than precisely locating it [29].

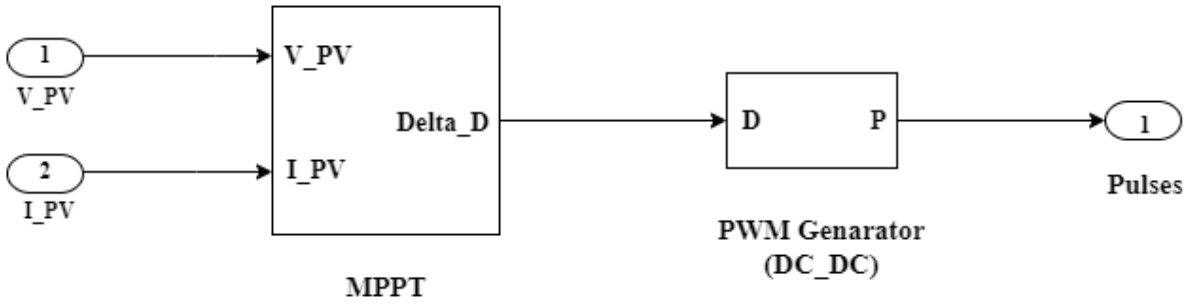

Figure 2.5: Block diagram of P&O

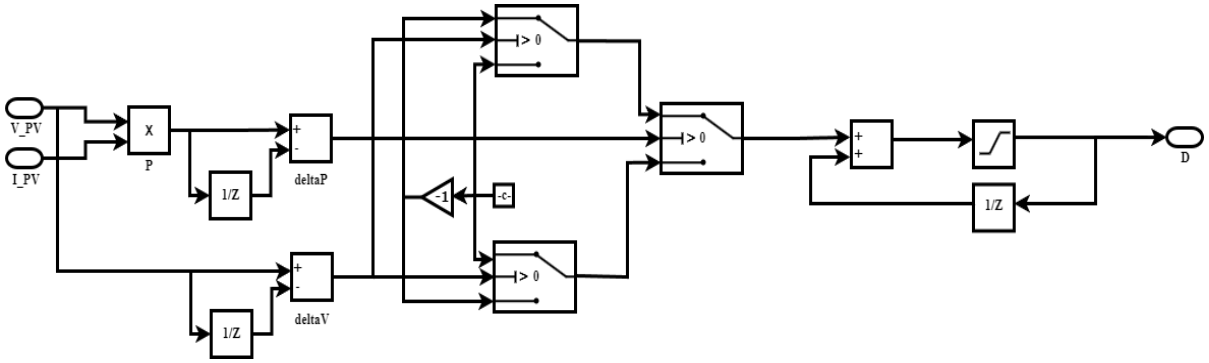

Figure 2.6: Block diagram of MPPT

2.2.5 DC-AC Inverter

The PV array produces DC energy, while the grid requires AC energy. To transfer the generated power to the grid, it must be converted into AC energy with controllable magnitude, phase, and frequency. To accomplish this, a three-phase voltage source inverter is utilized. The voltage source inverter (VSI) switches are controlled using space-vector pulse width modulation (SVPWM) [30]. The SVPWM technique is widely adopted for controlling voltage source inverters. Unlike sinusoidal pulse width modulation (SPWM), SVPWM is better suited for digital implementation and provides more efficient DC-link voltage utilization. Additionally, it effectively reduces total harmonic distortion (THD) [31].

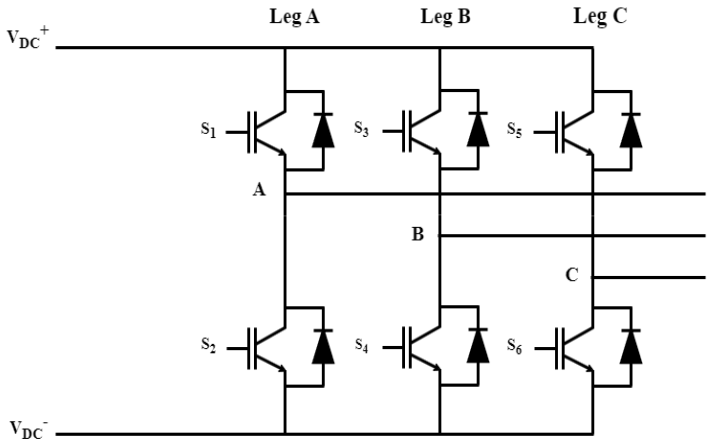

Figure 2.7: Three phase Inverter

Design of LCL-Filter

The LCL filter is implemented to reduce the high-frequency harmonics in the output current. The circuit diagram of the LCL filter is presented in Figure 2.8.

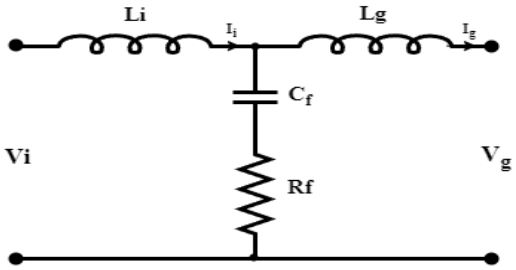

Figure 2.8: Circuit diagram of LCL filter

The design procedure for the LCL filter can be described by the following steps **[32],[35].**

Step 1: the filter capacitance is selected based on the limit of the reactive power absorbed by the capacitor. Generally, it should be less than 5% of the rated power. The value of capacitance is given by [33]:

$$C_f = XC_b \qquad (2.8)$$

Here, C_b represents the base capacitance, and X denotes the percentage of reactive power absorbed under rated conditions.

The base capacitance of the system can be determined using the following formula (2.9):

$$Z_b = \frac{V_{LLrms}^2}{P_{rated}} \qquad (2.9)$$

$$C_b = \frac{1}{2\pi f_g Z_b} \tag{2.10}$$

Where, V_{LLrms} represents the rms value of line-to-line voltage, P_{rated} represents the rated power of the system, Z_b represents the base impedance and f_g represents the grid frequency.

Step 2: The inverter-side inductor is utilized to minimize the ripple in the inverter current, and its value is determined based on the relationship between the ripple current and the inverter inductor [33]:

$$\Delta I = \frac{V_{DC}}{8 L_i F_s} \tag{2.11}$$

Where, ΔI represents the ripple current, usually limited from 10% to 20% of rated current, f_s represents switching frequency.

The ripple current of the inverter ΔI can be selected as 20% of base current. The base current I_b of the system is given by:

$$I_b = \frac{P_{rated}}{\sqrt{3} V_{LLrms}} \tag{2.12}$$

The inductor of the inverter side can be determined using the following formula (2.13):

$$L_i = \frac{V_{DC}}{8 f_s (20\%) I_b} \tag{2.13}$$

Step 3: The grid-side inductor can be determined based on the required ripple attenuation factor *RAF* at the switching frequency. *RAF* is the ratio between the grid current and the inverter output current, as follows:

$$RAF = \left| \frac{I_g(s)}{I_i(s)} \right| = \frac{\frac{1}{L_g C_f}}{s^2 + \frac{1}{L_g C_f}} \tag{2.14}$$

RAF at switching frequency is given by (P_{pev}) which can be rewritten as equation (2.15), (2-16) to calculate the grid inductor.

$$RAF_s = \left| \frac{I_g(s)}{I_i(s)} \right| = \frac{1}{1 - w_s^2 L_g C_f} \tag{2.15}$$

$$L_g = \left|\frac{I_g(s)}{I_i(s)}\right| = \frac{RAF_s + 1}{RAF_s w_s^2 C_f} \qquad (2.16)$$

Step 4: The resonance frequency should be kept well away from both the grid frequency and the switching frequency. The appropriate range for f_{res} is defined by the following equation (2.17) [32]:

$$f_{res} = \frac{1}{2\pi}\sqrt{\frac{L_g + L_i}{L_g L_i C_f}} \qquad (2.17)$$

$$10 f_g < f_{res} < \frac{f_s}{2}$$

Step 5: To prevent resonance phenomenon, a damping resistor R_f is usually placed in series with the filter capacitor. The value of the damping resistor can be determined using the following formula (2.18):

$$R_f = \frac{1}{3(2\pi f_{res} C_f)} \qquad (2.18)$$

Figure 2.9 illustrates the effect of the damping resistor on the transfer function of the LCL filter, showing the Bode plot of the filter without the damping resistor and demonstrating how the damping resistor effectively prevents resonance frequency in the filter.

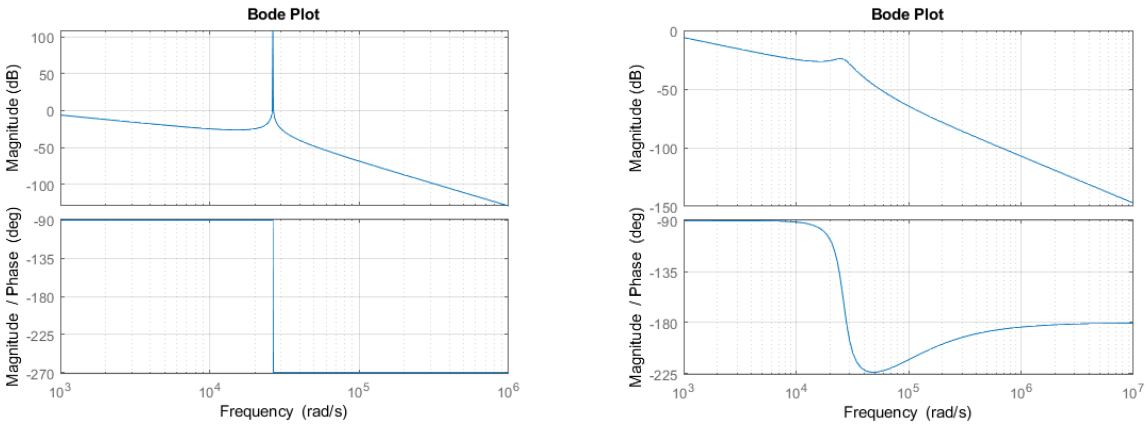

(a) (b)

Figure 2.9: Bode Plot of LCL filter: (a) without damping resistor (b) with damping resistor

Following the calculation of the inverter filter design parameters, these values are detailed in the table provided below.

Table 2.4: Inverter and grid parameters

Parameter name	Value
Inverter inductor (L_i)	$1.9e^{-3}$ [H]
Grid inductor (L_g)	$0.117e^{-3}$ [H]
Filter capacitor (C_f)	$12.992e^{-6}$ [F]
Damping resistor (R_f)	0.9707 [Ω]

The MATLAB code used to obtain the inverter and grid parameters are available in appendix A.

2.2.6 Space Vector PWM Strategy Control

Space-vector modulation (SVM) is a widely used real-time modulation technique for controlling voltage source inverters. The Space-Vector Pulse Width Modulation (SVPWM) technique is realized by rotating the reference vector through a state diagram that consists of six fundamental non-zero vectors arranged in a hexagonal configuration, as illustrated in Figure 2.10.

Principle of Space Vector PWM

To facilitate the analysis of PWM techniques, the values in the three-phase (*a-b-c)* coordinate system are commonly mapped to the α-β plane. In the SVPWM method, the reference voltage vector V_{ref}which rotates with a specific angular frequency, is used as the control command. The SVPWM approach involves identifying the sector, calculating the vector components, and determining the durations for the switching times [37].

Angle (α) and Reference Voltage Vector ($Vref$)

In the SVPWM, the three phase output voltage vector is represented by a reference vector that rotates at an angular speed of $\omega = 2\pi f$. The SVPWM approximates the reference vector by using combinations of different switching states. A reference voltage vector V_{ref}, rotating at an angular speed in the α-β plane, represents three sinusoidal waveforms with the same angular frequency in the coordinate system. The space vector with a magnitude of V_{ref} rotates in a circular path at an angular velocity, with the rotation direction depending on the phase sequence of the voltages. If the phase sequence is positive, it rotates counterclockwise. Otherwise, with a negative phase sequence, it rotates clockwise. The three-phase voltages can be represented using just two components, α and β, in a two-dimensional plane. The

magnitude of each active vector is $2\frac{V_{DC}}{3}$. The active vectors are separated and form the boundary of a hexagon. The trajectory of the circle projected by the space reference vector is determined by V_0,V_1,V_2, V_3, V_4,V_5,V_6 and V_7. According to the principle of space-vector PWM, the alpha-beta ($\alpha\beta$)-coordinate system can be represented by Clarke transformation using equation (2-19).

$$\begin{bmatrix} v_\alpha \\ v_\beta \end{bmatrix} = \frac{2}{3}\begin{bmatrix} 1 & -\frac{1}{2} & -\frac{1}{2} \\ 0 & \frac{\sqrt{3}}{2} & -\frac{\sqrt{3}}{2} \end{bmatrix} \times \begin{bmatrix} v_a \\ v_b \\ v_c \end{bmatrix} \qquad (2.19)$$

The 3-phase quantities are reduced to two phase quantities, the first one is direct axis (real axis) and other one is quadrature axis (imaginary axis). These two quantities are represented as the magnitude (V_{ref}) and angle (α). V_{ref} rotates with the speed of angular velocity ω = $2\pi f$. SVPWM combines the reference voltage with six switching states of the inverter. As depicted in Figure 2.10, the basic switching vectors and sector diagram form a hexagon divided into six sectors of 60^oeach. The reference vector, which represents three-phase sinusoidal voltage, is generated by switching between two adjacent active vectors and zero vectors using SVPWM [38].

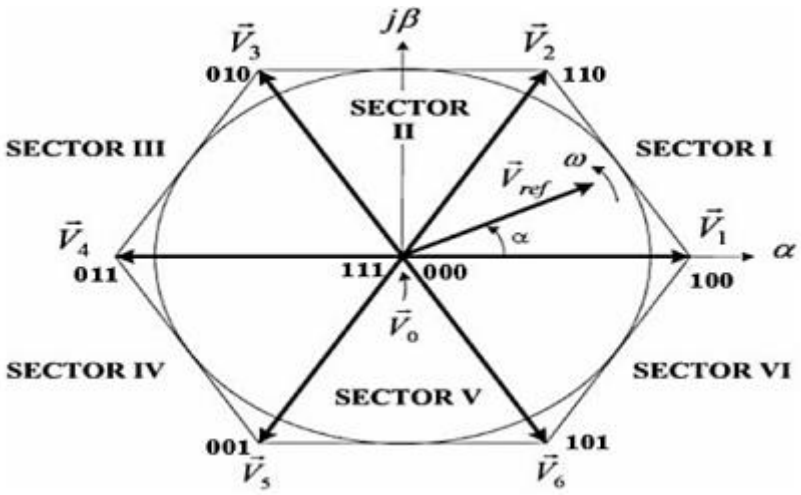

Figure 2-10: Representation of space vector in complex plane [38]

The magnitude of the reference voltage and the angle required for implementing SVPWM are determined as follows:

$$|V_{ref}| = \sqrt{v_\alpha^2 + v_\beta^2} \qquad (2.20)$$

$$\alpha = \tan^{-1}\left(\frac{v_\beta}{v_\alpha}\right)$$

Determination of Sector

It is crucial to identify the sector where the reference output voltage is located to determine the switching time and sequence accurately. The phase voltages are associated with eight switching states: six nonzero vectors and two zero vectors at the origin. Based on the reference voltage and the angle of the reference vector, the sector can be determined, as illustrated in Table 2.5.

Table 2.5: Sector Identification

Sector	Degrees
1	$0 < \alpha \leq 60^o$
2	$60^o < \alpha \leq 120^o$
3	$120^o < \alpha \leq 180^o$
4	$180^o < \alpha \leq 240^o$
5	$240^o < \alpha \leq 300^o$
6	$300^o < \alpha \leq 360^o$

Determination of the Switching Times for each transistor

To minimize the switching frequency for each inverter leg, it's necessary to arrange the switching sequence carefully. There are multiple switching patterns available for implementing SVPWM, but to reduce switching losses, only two adjacent active vectors and two zero vectors are used within a sector. To achieve this optimal condition, each switching period begins with one zero vector and ends with another zero vector within the sampling time. This approach generally applied to three-phase inverters as a switching sequence. As a result, the switching cycle of the output voltage is twice the sampling time, leading to symmetrical output voltage waveforms. A symmetric switching sequence is shown in Table 2.6 [37].

Table 2.6: Segment switching sequences

Space vector	Switching state	On state switch	Off state switch	Vector definition
V_0	000	S_4, S_6, S_2	S_1, S_3, S_5	$V_0 = 0$
V_1	100	S_1, S_6, S_2	S_4, S_3, S_5	$V_1 = \frac{2}{3} V_{DC}$
V_2	110	S_1, S_3, S_2	S_4, S_6, S_5	$V_2 = \frac{2}{3} V_{DC} e^{-i\frac{\pi}{3}}$
V_3	010	S_4, S_3, S_2	S_1, S_6, S_5	$V_3 = \frac{2}{3} V_{DC} e^{-i\frac{2\pi}{3}}$
V_4	011	S_4, S_3, S_5	S_1, S_6, S_2	$V_4 = \frac{2}{3} V_{DC} e^{-i\frac{3\pi}{3}}$
V_5	001	S_4, S_6, S_5	S_1, S_3, S_2	$V_5 = \frac{2}{3} V_{DC} e^{-i\frac{4\pi}{3}}$
V_6	101	S_1, S_6, S_5	S_4, S_3, S_2	$V_6 = \frac{2}{3} V_{DC} e^{-i\frac{5\pi}{3}}$
V_7	111	S_1, S_3, S_5	S_4, S_6, S_2	$V_7 = \frac{2}{3} V_{DC}$

According to this table, the binary forms of two neighboring basic vectors vary by just one bit. Therefore, when transitioning from one vector to its adjacent one, only one of the upper transistors' switches closes. The output voltage is produced by time-averaging the two vectors during a sample period. To determine the duration for applying different vectors, refer to Figure 2.11, which shows the positions of the available space vectors and the reference vector within the first sector.

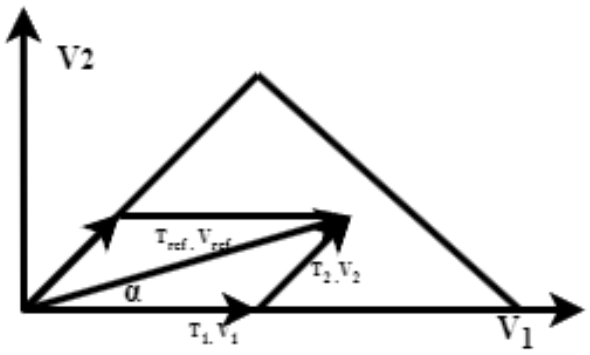

Figure 2.11: Principle of space vector time calculation

The duration of each active phase vector can be determined as follows:

$$T_1 = \sqrt{3}\frac{V_{ref}}{V_{DC}} T_s \sin\left(\frac{n\pi}{3} - \alpha\right) \qquad (2.21)$$

$$T_2 = \sqrt{3}\frac{V_{ref}}{V_{DC}} T_s \sin\left(\alpha - \frac{(n-1)\pi}{3}\right) \qquad (2.22)$$

$$T_0 = T_s - T_1 - T_2$$

Where n denotes the number of sectors.

2.3 Grid Connected PV System

2.3.1 Control Structure of Grid Connected Inverter

The control system of a grid-connected inverter is responsible for regulating the injection of power into the grid, derived from a distributed generator. This is generally achieved through control structures that utilize two sequential control loops. Various combinations of cascaded loops can be implemented, including an outer power loop and an inner current loop and outer voltage and inner power loop. But the most widely used strategy as mentioned in **[**9] is the approach that utilizes a slower outer DC-link voltage control loop in conjunction with a faster inner current control loop.

The voltage control loop manages the balance of power flow within the system. When there is excess power from the DC side, this loop's controller adjusts the reference current to increase the AC power output to the grid. Conversely, the current control loop is responsible for maintaining the quality of power and reducing harmonics present in the inverter's current, ensuring that it can be effectively integrated into the grid.

The control system can be configured using one of three reference frames: the natural reference frame, the stationary reference frame, or the synchronous reference frame. In the natural reference frame, it is necessary to have an individual controller for each phase current [34]. Since the currents are sinusoidal, non-linear controllers such as deadbeat and hysteresis are employed in the natural reference frame.

In the stationary reference frame control implementation, the abc variables are converted into αβ-axis variables. These variables are also sinusoidal. Proportional-Resonant (PR) controllers are commonly used in this frame because PI controllers are unable to eliminate steady-state errors in sinusoidal signals [9]. One possible implementation of control structure in stationary reference frame is depicted in Figure 2.12.

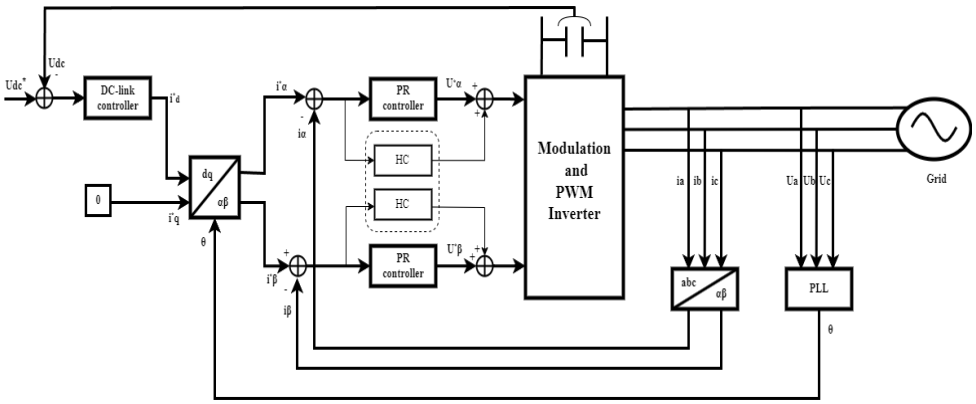

Figure 2.12: General structure for implementation of control in stationary RF

In the synchronous reference frame, sinusoidal variables are transformed into a rotating frame that moves at synchronous speed, causing these variables to appear as DC values. As a result, PI controllers can be utilized, as they are effective for handling DC quantities [9]. Figure 2.13 shows general control structure in synchronous reference frame (SRF).

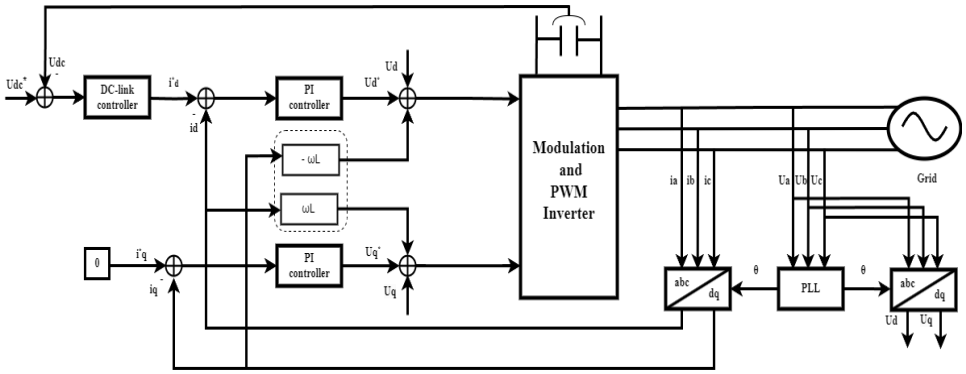

Figure 2.13: General control structure in synchronous reference frame

2.3.2 Control Structure of the Inverter

The primary focus of the system is not just to achieve the highest power output from the PV array, but to effectively control the inverter to regulate both active and reactive power flow. The inverter's control structure manages all aspects, including grid synchronization, power flow regulation, and pulse width modulation. In this model, the control going to be used is synchronously rotating reference frame which is used to transform voltage and current quantities from natural reference frame (*abc*-frame) to synchronously rotating reference frame (dq-frame).

2.3.2.1 Representation of Three Phase Variables in Stationary RF

It converts three-phase abc signals into a two-phase orthogonal system within a stationary reference frame, where the α and β axes are maintained in a fixed position by the transformation. This transformation is commonly utilized in the analysis of electrical machines and the control of power electronic converters because it simplifies operations by reducing the number of signals involved. The transformation from natural reference frame (abc-frame) to stationary reference frame (αβ-frame) is given in matrix form as follows [41].

$$\begin{bmatrix} i_\alpha \\ i_\beta \\ i_0 \end{bmatrix} = \frac{2}{3}\begin{bmatrix} 1 & -\frac{1}{2} & \frac{1}{2} \\ 0 & \frac{\sqrt{3}}{2} & -\frac{\sqrt{3}}{2} \\ \frac{1}{2} & \frac{1}{2} & \frac{1}{2} \end{bmatrix} \times \begin{bmatrix} i_a \\ i_b \\ i_c \end{bmatrix} \qquad (2.23)$$

$$\begin{bmatrix} v_\alpha \\ v_\beta \\ v_0 \end{bmatrix} = \frac{2}{3}\begin{bmatrix} 1 & -\frac{1}{2} & \frac{1}{2} \\ 0 & \frac{\sqrt{3}}{2} & -\frac{\sqrt{3}}{2} \\ \frac{1}{2} & \frac{1}{2} & \frac{1}{2} \end{bmatrix} \times \begin{bmatrix} v_a \\ v_b \\ v_c \end{bmatrix} \qquad (2.24)$$

The scaling factor $2/3$ is being considered for amplitude invariant transformations. In a balanced three phase systems, $I_a + I_b + I_c = 0$ andI_0can be neglected, which is resulting in simplified transformation form as follows,

$$\begin{bmatrix} i_\alpha \\ i_\beta \end{bmatrix} = \frac{2}{3}\begin{bmatrix} 1 & -\frac{1}{2} & \frac{1}{2} \\ 0 & \frac{\sqrt{3}}{2} & -\frac{\sqrt{3}}{2} \end{bmatrix} \times \begin{bmatrix} i_a \\ i_b \\ i_c \end{bmatrix} \qquad (2.25)$$

From the three phase currents, the αβ current components can be calculated as can be seen in (2.25), and the αβ components of the voltages can be calculated from line-to-line voltages using (2.26)

$$\begin{bmatrix} v_\alpha \\ v_\beta \end{bmatrix} = \frac{2}{3}\begin{bmatrix} 1 & -\frac{1}{2} & \frac{1}{2} \\ 0 & \frac{\sqrt{3}}{2} & -\frac{\sqrt{3}}{2} \end{bmatrix} \times \begin{bmatrix} v_a \\ v_b \\ v_c \end{bmatrix} \qquad (2.26)$$

The simplified inverse Clarke transformation used to convert quantities back to the natural reference frame (abc-frame) is given as:

$$\begin{bmatrix} i_a \\ i_b \\ i_c \end{bmatrix} = \frac{3}{2}\begin{bmatrix} \frac{2}{3} & 0 \\ -\frac{1}{3} & \frac{1}{\sqrt{3}} \\ -\frac{1}{3} & -\frac{1}{\sqrt{3}} \end{bmatrix} \times \begin{bmatrix} i_\alpha \\ i_\beta \end{bmatrix} \qquad (2.27)$$

$$\begin{bmatrix} v_a \\ v_b \\ v_c \end{bmatrix} = \frac{3}{2}\begin{bmatrix} \frac{2}{3} & 0 \\ -\frac{1}{3} & \frac{1}{\sqrt{3}} \\ -\frac{1}{3} & -\frac{1}{\sqrt{3}} \end{bmatrix} \times \begin{bmatrix} v_\alpha \\ v_\beta \end{bmatrix} \qquad (2.28)$$

2.3.2.2 Representation of Three Phase Variables in SRRF

In a stationary rotating reference frame, three-phase signals change over time since the frame is fixed. To achieve a time-invariant representation of these signals, it is necessary for the reference frame to rotate synchronously with the rotating space vector. This concept, known as the dq-synchronous reference frame, was proposed by Park in (1929) for the analysis of synchronous machines. The transformations from abc-frame to dq0-frame is given as [41].

$$\begin{bmatrix} i_d \\ i_q \\ i_0 \end{bmatrix} = \frac{2}{3}\begin{bmatrix} cos\,\omega t & \cos(\omega t - \frac{2\pi}{3}) & \cos(\omega t + \frac{2\pi}{3}) \\ -\sin\omega t & -\sin(\omega t - \frac{2\pi}{3}) & -\sin(\omega t + \frac{2\pi}{3}) \\ \frac{1}{2} & \frac{1}{2} & \frac{1}{2} \end{bmatrix} \times \begin{bmatrix} i_a \\ i_b \\ i_c \end{bmatrix} (2.29)$$

$$\begin{bmatrix} v_d \\ v_q \\ v_0 \end{bmatrix} = \frac{2}{3}\begin{bmatrix} cos\,\omega t & \cos(\omega t - \frac{2\pi}{3}) & \cos(\omega t + \frac{2\pi}{3}) \\ -\sin\omega t & -\sin(\omega t - \frac{2\pi}{3}) & -\sin(\omega t + \frac{2\pi}{3}) \\ \frac{1}{2} & \frac{1}{2} & \frac{1}{2} \end{bmatrix} \times \begin{bmatrix} v_a \\ v_b \\ v_c \end{bmatrix} (2.30)$$

Where $\theta = \omega t$ is the reference phase angle. This transformation requires the information of the reference phase angle. The phase angle information can be obtained by using the phase locked loop (PLL).

Since the system is balanced, the above equation (2.29) and equation (2.30) are simplified in the following transformation matrix form as follows,

$$\begin{bmatrix} i_\alpha \\ i_\beta \end{bmatrix} = \frac{2}{3}\begin{bmatrix} cos\,\omega t & \cos(\omega t - \frac{2\pi}{3}) & \cos(\omega t + \frac{2\pi}{3}) \\ -\sin\omega t & -\sin(\omega t - \frac{2\pi}{3}) & -\sin(\omega t + \frac{2\pi}{3}) \end{bmatrix} \times \begin{bmatrix} i_a \\ i_b \\ i_c \end{bmatrix} (2.31)$$

$$\begin{bmatrix} v_\alpha \\ v_\beta \end{bmatrix} = \frac{2}{3}\begin{bmatrix} cos\,\omega t & \cos(\omega t - \frac{2\pi}{3}) & \cos(\omega t + \frac{2\pi}{3}) \\ -\sin\omega t & -\sin(\omega t - \frac{2\pi}{3}) & -\sin(\omega t + \frac{2\pi}{3}) \end{bmatrix} \times \begin{bmatrix} v_a \\ v_b \\ v_c \end{bmatrix} (2.32)$$

The inverse Park transformation from dq0-frameto *abc*-frame is provided as follows,

$$\begin{bmatrix} i_a \\ i_b \\ i_c \end{bmatrix} = \frac{3}{2}\begin{bmatrix} cos\,\omega t & -\sin\omega t \\ \cos(\omega t - \frac{2\pi}{3}) & -\sin(\omega t - \frac{2\pi}{3}) \\ \cos(\omega t + \frac{2\pi}{3}) & -\sin(\omega t + \frac{2\pi}{3}) \end{bmatrix} \times \begin{bmatrix} i_d \\ i_q \end{bmatrix} \quad (2.33)$$

$$\begin{bmatrix} v_a \\ v_b \\ v_c \end{bmatrix} = \frac{3}{2}\begin{bmatrix} cos\,\omega t & -\sin\omega t \\ \cos(\omega t - \frac{2\pi}{3}) & -\sin(\omega t - \frac{2\pi}{3}) \\ \cos(\omega t + \frac{2\pi}{3}) & -\sin(\omega t + \frac{2\pi}{3}) \end{bmatrix} \times \begin{bmatrix} v_d \\ v_q \end{bmatrix} \quad (2.34)$$

In this thesis, the αβ to abc and dq0 to *abc* transformation supports space vector pulse width modulation (SVPWM) by generating the necessary pulse signals for the inverter's switching, thus facilitating the control of the voltage source inverter (VSI).

2.3.2.3 Grid Synchronization

The phase information of the grid voltage can be derived using a phase-locked loop (PLL). This information is critical for synchronizing the three-phase inverter current with the grid voltage. It provides the necessary phase angle for the dq transformation of both current and voltage, thereby ensuring that the magnitudes of the grid voltage and the inverter's output are matched.

2.3.2.4 Control Loops for Inverter Control

Inverter systems utilize a dual-loop control strategy, consisting of an outer voltage control loop and an inner current control loop. The outer loop is responsible for controlling the DC-link voltage, while the inner loop regulates the current supplied to the grid. A Proportional-Integral (PI) controller is typically used for voltage regulation, whereas both PI

and Proportional-Resonant (PR) controllers are utilized for managing the current. To optimize these controllers' performance, Particle Swarm Optimization (PSO) is used to fine-tune their parameters, enhancing stability and accuracy in the system [42].

PI Controller-Based Outer Voltage Control

The outer voltage control loop plays a critical role in maintaining the DC-link voltage stability in a three-phase grid-connected inverter system. The DC-link voltage acts as an energy buffer between the DC side (generated by the solar PV system) and the AC side (delivered to the grid). Ensuring this voltage remains stable is essential for consistent power flow from the solar system to the grid, even when solar irradiance or grid conditions vary [43]. Instability in the DC-link voltage can lead to disruptions in power transfer and degrade inverter performance. By regulating the DC-link voltage, the outer voltage loop controls the system's energy balance, ensuring that the power drawn from the PV system is consistently matched with the power delivered to the grid. Proper regulation of the DC-link voltage is critical for grid synchronization and for efficient, safe power delivery [44].

The Proportional-Integral (PI) controller in the outer voltage loop regulates the DC-link voltage by minimizing the difference between the measured voltage and a reference voltage, referred to as the voltage error. It achieves this by adjusting two main parameters: the Proportional Gain (K_p), which reacts to the magnitude of the error to provide a quick corrective action, and the Integral Gain (K_i), which addresses long-term errors by accumulating the voltage error over time, helping to eliminate steady-state deviations. The PI controller manages the voltage error to produce a reference current, which is sent to the inner current control loop. This reference current ensures the inverter delivers the necessary power to maintain the stability of the DC-link voltage. The inner current loop then regulates the actual current flowing into the grid based on the reference generated by the outer voltage loop [45]. Figure 2.14 shows the outer voltage loop.

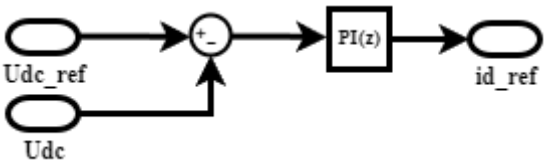

Figure 2.14: The outer voltage loop

PI and PR Controllers for Inner Current Control

The inner current loop in a three-phase grid-connected inverter system ensures accurate control of the inverter's output current by tracking the reference current set by the outer voltage loop, which is based on the desired grid current and voltage command. This ensures that the actual current matches with the reference for precise power delivery to the grid. Additionally, the inner current loop aids in maintaining grid synchronization by quickly adjusting the inverter's output to correct any deviations, preventing phase misalignment and enhancing system stability.

The transfer function of a PI controller [46]:

$$G_{PI}(s) = K_p + \frac{K_i}{s} \qquad (2.35)$$

where:

- K_p is the proportional gain
- K_i is the integral gain

The PI (Proportional-Integral) controller is widely used in the dq-reference frame to manage both the outer voltage and inner current loops in grid-connected inverter systems, with a focus on controlling active and reactive power. Within the outer voltage loop, the PI controller regulates the DC-link voltage and sets the reference for the inner current loop. By transforming three-phase currents into direct d and quadrature q components, the dq reference frame simplifies control. The d-axis, which aligns with the grid voltage, is responsible for controlling active power, whereas the q-axis handles reactive power. To ensure that only active power is supplied to the grid, the q-axis current is typically set to zero, preventing reactive power generation [47], Two PI controllers are adopted to regulate I_d and I_q according to the current references I_d^* and I_q^*. The PI controller adjusts the inverter output by minimizing the error between the reference and measured currents, with the proportional part responding to immediate deviations and the integral part addressing steady-state errors, thus improving tracking accuracy [9]. Figure 2.15 depicts the Simulink model of the current and voltage controller of grid connected PV inverter.

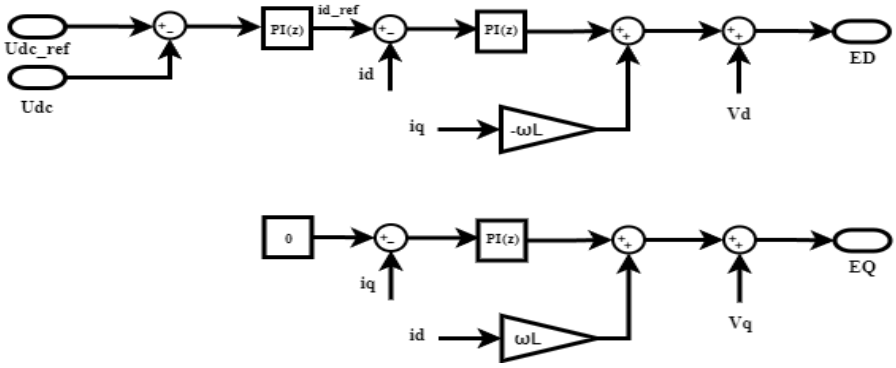

Figure 2.15: Current control loop using PI controller

PR Controller for Inner Current Control

The Proportional-Resonant (PR) controller plays a crucial role in improving the current tracking, especially for sinusoidal reference currents in grid-connected applications. Traditional PI controllers are effective for regulating DC signals but struggle with AC signals, leading to steady-state errors in sinusoidal current tracking. The PR controller addresses this limitation by providing excellent performance for sinusoidal currents through the introduction of a resonant term.

The PR controller is specifically developed to manage periodic AC signals by offering infinite gain at the grid frequency, ensuring zero steady-state error when tracking sinusoidal reference signals. This is particularly important in grid-tied systems, where precise current injection is required to meet strict grid standards.

The control transfer function of the PR controller is represented as [46]:

$$G_{PR}(s) = K_p + \frac{K_r s}{{\omega_0}^2 + s^2} \qquad (2.36)$$

where:

- K_p is the proportional gain
- K_r is the resonant gain
- ω_0 is the angular frequency of the AC signal.

A PR controller is usually adopted in the stationary reference αβ frame for inverter control. The block diagram of a current-controlled VSI in the stationary reference frame with the PR controller is shown in Figure 2.16. The three-phase currents are transformed into αβ components I_α and I_β using the $abc \rightarrow$ αβ transformation. The a component corresponds to

the Phase α component, while the β component represents a combination of the Phase b and Phase c components (assuming the currents are balanced). Therefore, it is sufficient to control just two current channels, I_α and I_β, using two separate PR controllers. The PR controllers, typically paired with the harmonic compensator to ensure that I_α and I_β follow the reference currentsI_α^*, and I_β^*. He resulting output from the PR controllers is then converted back into the abc frame and subsequently turned into PWM signals to operate the switches [48].

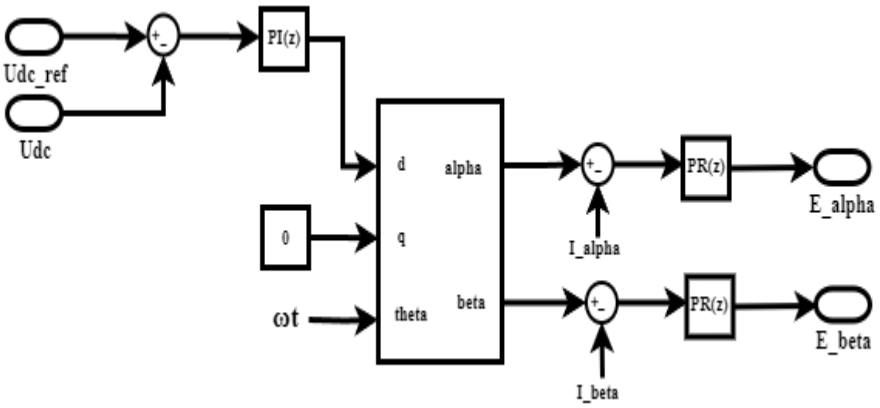

Figure 2.16: Current control loop using PR controller

PSO Optimization for PI Parameters

To enhance the performance of the PI and PR controller, optimization techniques such as Particle Swarm Optimization (PSO) can be employed to fine-tune the proportional and integral gains (K_p and K_i), and the proportional and resonant gains (K_p and K_r). PSO, a nature-inspired algorithm that simulates social behaviors like flocking or schooling, effectively explores the parameter space to find optimal values. This includes reducing voltage overshoot during sudden load changes, improving the transient response to achieve rapid stabilization after perturbations, and minimizing steady-state error for a more accurate results. Utilizing PSO allows the PI and PR controller to automatically find the most effective gains for improved performance, minimizing the need for manual adjustments and ensuring efficient system response under diverse conditions [49].

2.3.3 Block Diagram of Overall System

Previously, we modeled the core components of the grid-connected PV inverter system. These components include the PV array, the DC-DC boost converter with an MPPT controller using Perturb and Observe (P&O), the voltage source inverter (VSI) with an LCL filter, the phase-locked loop (PLL) and the VSI controller. Figure 2.17 shows the

MATLAB/SIMULINK model for the grid-connected PV system, which comprises the following parts described below.

PV Array: the PV array consists of one parallel string and two series strings that each string consisting of 66 modules which are connected in series. The PV array can generate a maximum power of $800\,[W]$ at a constant solar irradiance $G = 1000\,[W/m^2]$ and temperature $T = 25^o[C]$.

DC-DC Boost Converter: the boost converter is used to enhance the maximum voltage of the PV array from $76\,[V]$ to the appropriate voltage level that is $200\,[V]$. The duty cycle of the boost converter is generated by MPPT using P&O block diagram. The boost converter is operated at the switching frequency of $5\,[KHz]$.

MPPT Controller: uses the Perturb and Observe blocks to generate the duty cycle of the boost converter. This controller automatically varies the duty cycle of the converter in order to extract the maximum power from the PV array.

Voltage Source Inverter: The two levels IGBT voltage source inverter is used to convert the $200\,[V]$ DC-link voltage to the line-to-line rms AC voltage of $70\,[V]$. The inverter switches are controlled by using the space vector pulse width modulation (SVPWM) technique. So, the space vector pulse width modulation signals are generated by the inverter controller. The voltage source inverter controller is used to generate the appropriate gate signals for the voltage source inverter switch to generate the required AC voltage and current.

Inverter with SVPWM and Grid Filter: an LCL-filter is very important to reduce the total harmonics which is produced by the voltage source inverter.

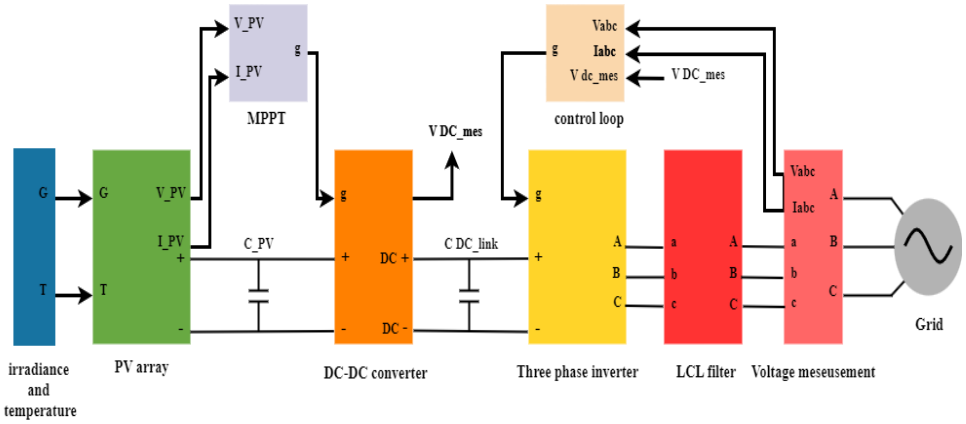

Figure 2.17: The Complete Model of the Grid Connected PV System

2.3 Conclusion

This chapter covered the key components and control strategies of a grid-connected photovoltaic system. It began with the basics of photovoltaic cells and the modeling of PV modules. The design of the DC-DC boost converter and the Perturb & Observe MPPT method were explored for maximizing energy output. The DC-AC inverter, LCL filter design for harmonic reduction, and the Space Vector PWM control technique were then discussed. The second section focused on the inverter's control structure, including three-phase variable representation, grid synchronization, and control loops for stable operation. A block diagram of the overall system concluded the chapter, summarizing the discussed concepts.

Chapter 3
Simulation and Results

3.1 Introduction

This chapter presents the results obtained from the model designed in chapters 1 and 2. It shows all the simulations for the DC-DC boost converter with the MPPT controller, the reduction of the inverter's THD and the inverter control scheme, and the overall system's results under different atmospheric conditions. The complete grid-connected PV model and simulation results were done utilizing MATLAB/SIMULINK.

3.2 Analysis of DC/DC converter behavior

This section analyzes the performance of the DC/DC converter connected to the PV array under different irradiation levels. The converter is designed to boost the PV array's output voltage to approximately 200 [V] and employs Maximum Power Point Tracking (MPPT) using Perturb and Observe blocks diagram integrated into the boost converter. By adjusting the irradiation levels from $1000\,[W/m^2]$ to $500\,[W/m^2]$, and subsequently to $300\,[W/m^2]$, we assess the corresponding changes in PV output power (P_{PV}) and voltage (V_{PV}). As shown in Figure 2.3 in the previous chapter, the PV array reaches its maximum power with the highest P_{PV} and V_{PV} at $1000\,[W/m^2]$. With decreased irradiation, both P_{PV}, I_{PV} and V_{PV} correspondingly drop, underscoring the significant influence of irradiation levels on the converter's performance in maximizing power extraction. The following results represented in Figure 3.1 show that the DC-DC converter effectively responds to varying environmental conditions.

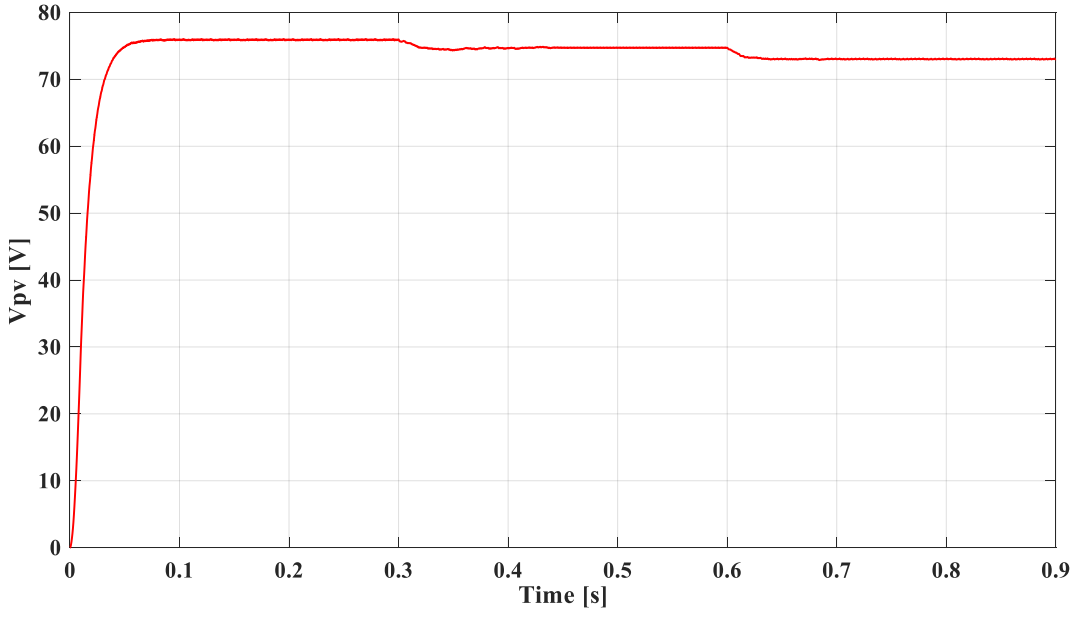

(a)

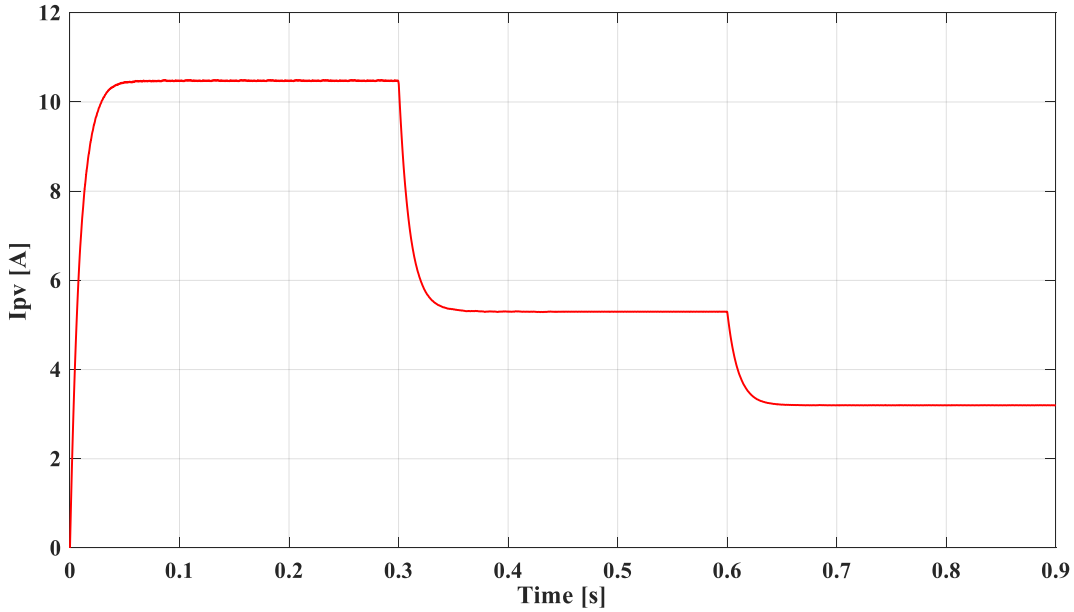

(b)

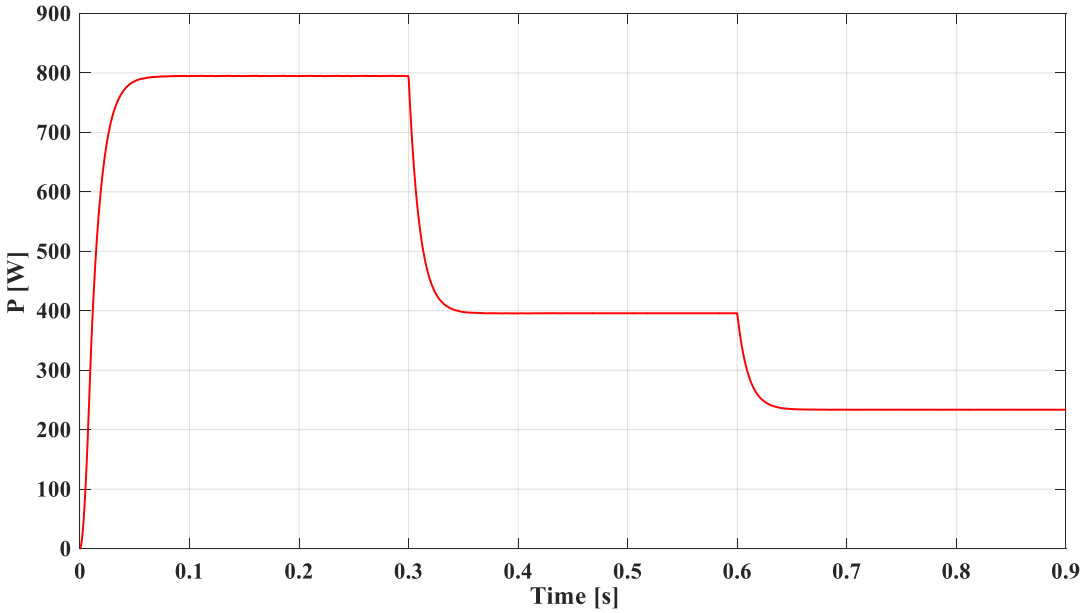

(c)

Figure 3.1: V_{PV},I_{PV} and P_{PV} Outputs of DC-DC converter under different assumed irradiance scenarios: (a) V_{PV} , (b) I_{PV} , (c) P_{PV}

3.3 DC-Link Voltage

The DC-link voltage is regulated by a voltage controller, which ensures that the power from the PV array is nearly equal to the power supplied to the grid. As shown in Figure 3.2, the DC-link voltage and the reference voltage signal for the controller are shown. While changes in irradiance or temperature can cause minor fluctuations in the DC-link voltage, the controller adjusts it to maintain the desired level. The DC-link voltage tracks the reference

voltage signal within an acceptable range, as shown in Figure 3.3, where the error between the DC-link voltage and the reference voltage is nearly zero.

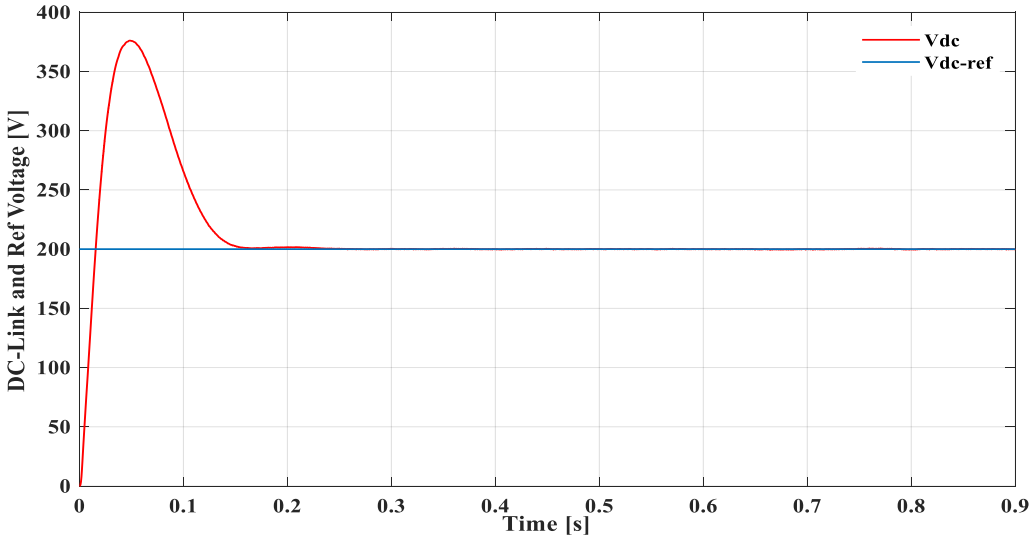

Figure 3.2: DC-link voltage and reference voltage signal outputs

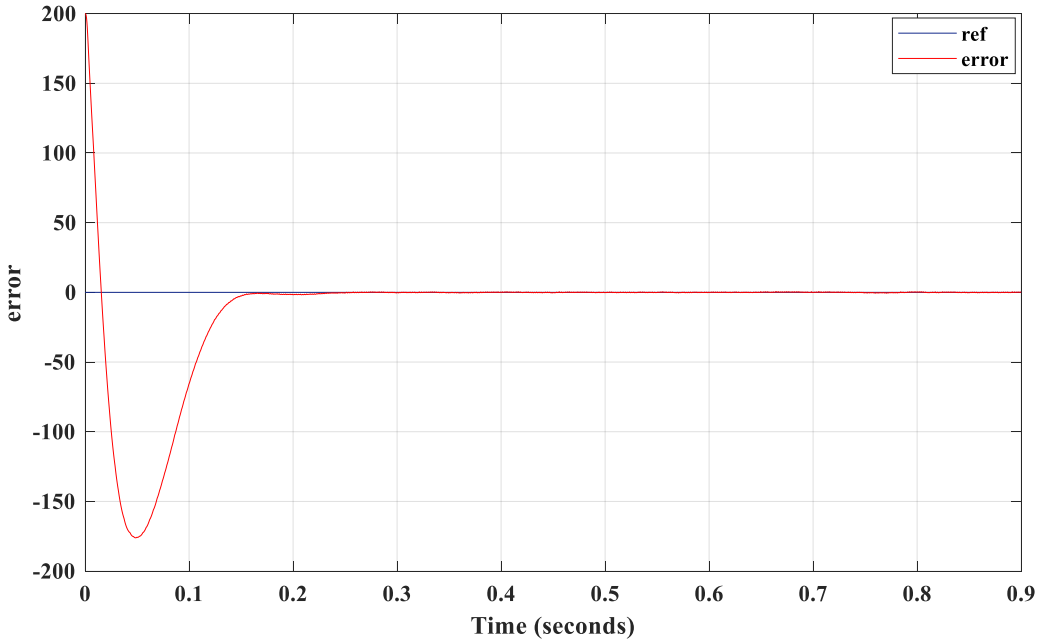

Figure 3.3: Error signal between DC-link voltage and reference voltage.

The value of PI controller parameters obtained from PSO algorithm is shown in Table 3.1

Table 3.1: Parameters of the PI controller for the outer voltage loop

Parameter	Value
K_p	0.05
K_i	1

3.4 Analysis of DC/AC Grid connected converter behavior

The inverter converts the DC voltage from the boost converter into AC signals. This AC signal is a two-level signal, with the line-to-line voltage oscillating between the positive and negative values of the DC-link voltage, as depicted in Figure 3.4.

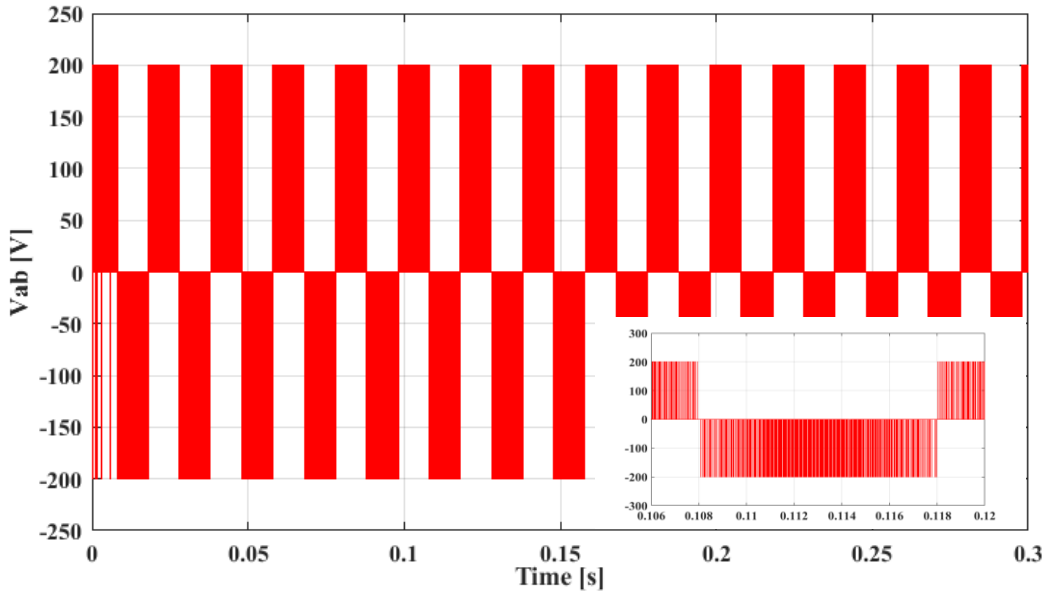

Figure 3.4: Inverter output voltage V_{ab}

Voltage source inverters often introduce disturbances that can affect the entire grid-connected PV system and degrade its power quality. To prevent this, an LCL filter is utilized to reduce high-frequency harmonics and meet standard requirements. Figures 3.5 and 3.6 demonstrate how the LCL filter helps mitigate disturbances in the inverter's current and voltage. The results of the inverter's output current and voltage with the FFT spectrum are shown in Figures 3.7 and 3.8, respectively.

Before filtering:

The results below illustrate the voltage output waveforms in Figure 3.5 and the current in Figure 3.7 without filtering. We can see that the phase-to-neutral voltage waveform resembles a staircase; this type of waveform is known to reduce the total harmonic distortion and push the noise to higher frequencies, making the filtering process easier and more efficient.

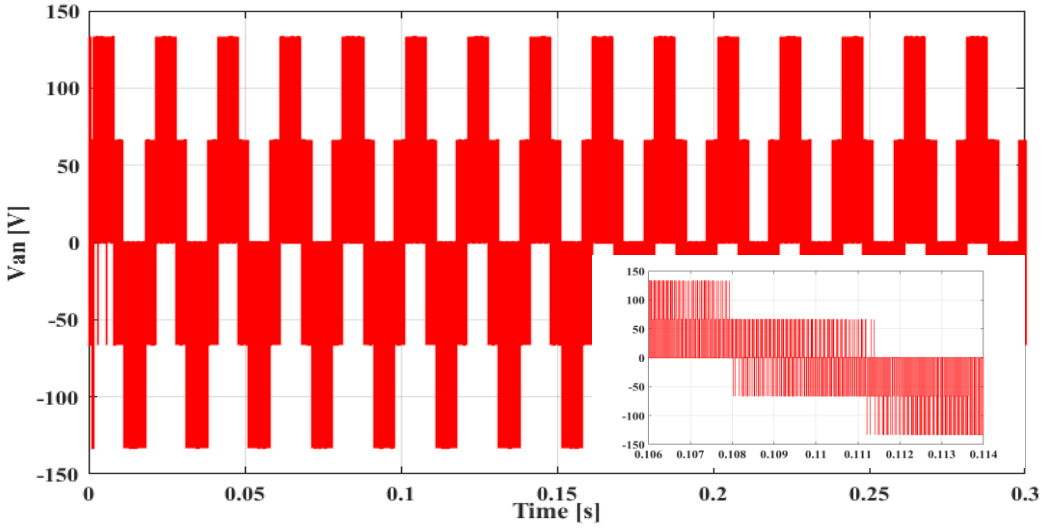

Figure 3.5: Unfiltered output voltage waveform of the inverter.

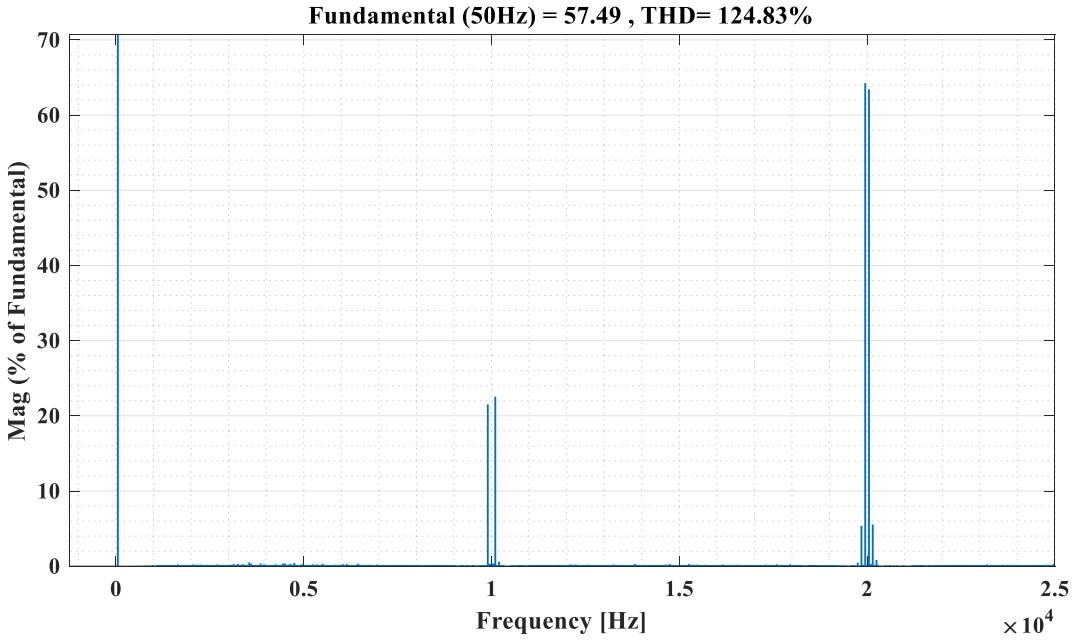

Figure 3.6: FFT analysis of inverter output voltage before filtering.

Figure 3.6 represents the Fast Fourier Transform that decomposes our signal into a sum of sinusoidal signals with the corresponding amplitude and frequency. Our waveforms consist of many high-frequency harmonics as multiples of the switching frequency, with relatively high amplitude starting from 10[kHz]. As a result, the fundamental frequency only represents 54 of the total amplitude.

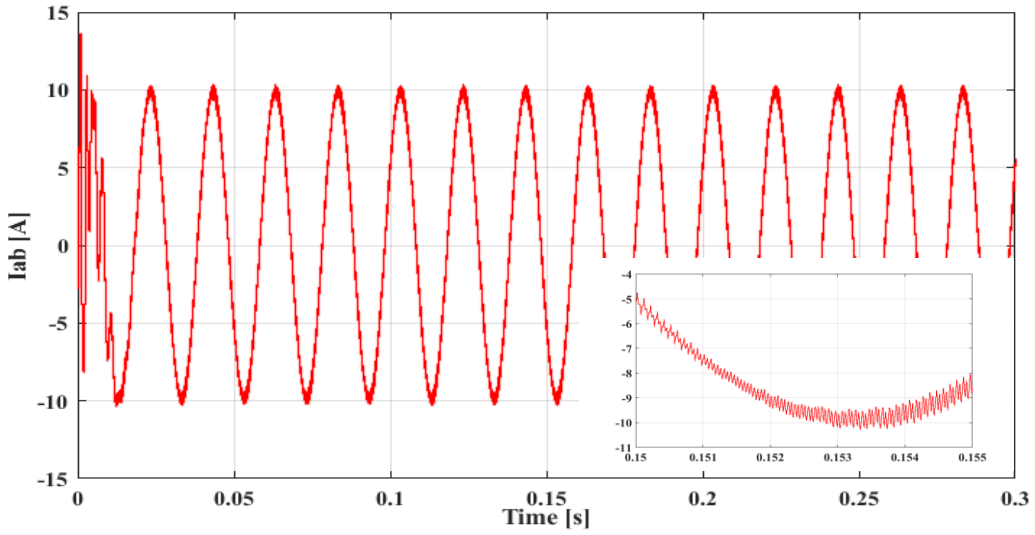

Figure 3.7: Unfiltered output current waveform of the inverter.

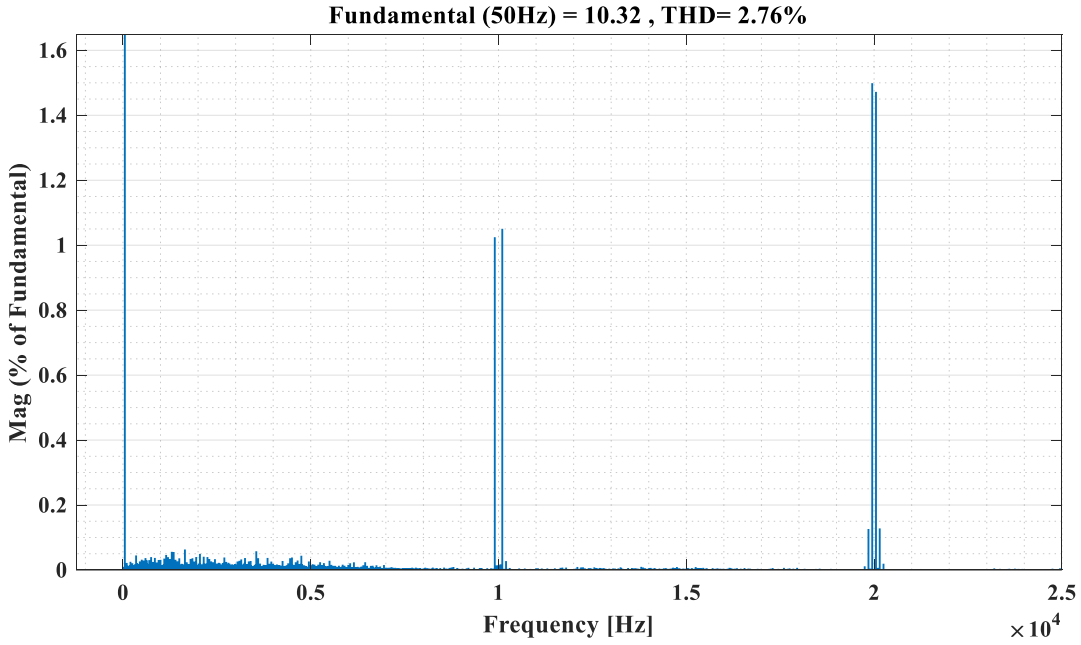

Figure 3.8: FFT analysis of inverter output current before filtering.

Unlike the voltage, the current has a lower THD due to the presence of the grid inductance, which acts as a low-pass filter.

After filtering:

The results presented below illustrate the output waveforms of voltage in Figure 3.9 and current in Figure 3.12 before the application of filtering.

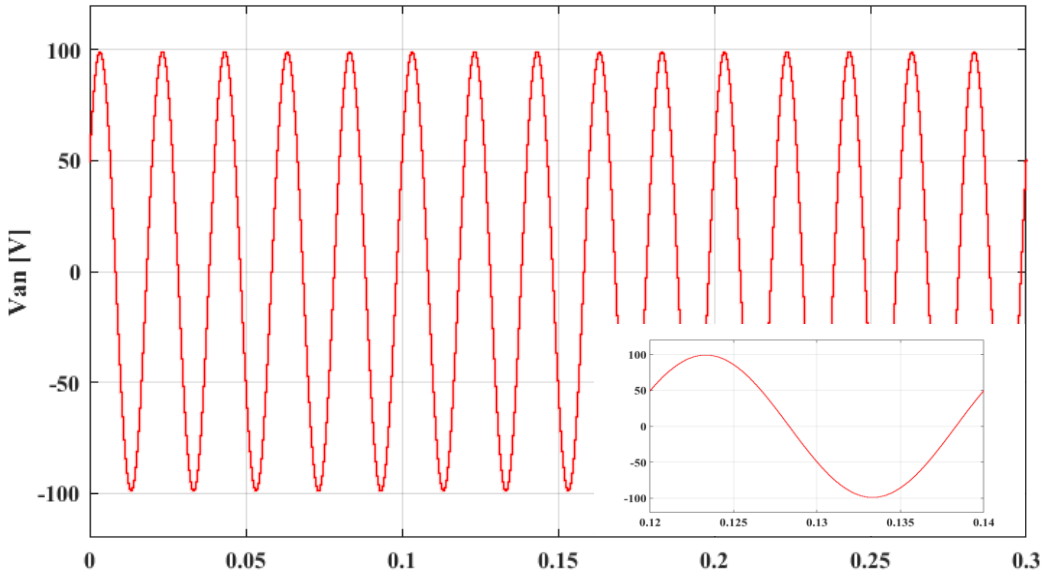

Figure 3.9: Filtered output voltage waveform of the inverter

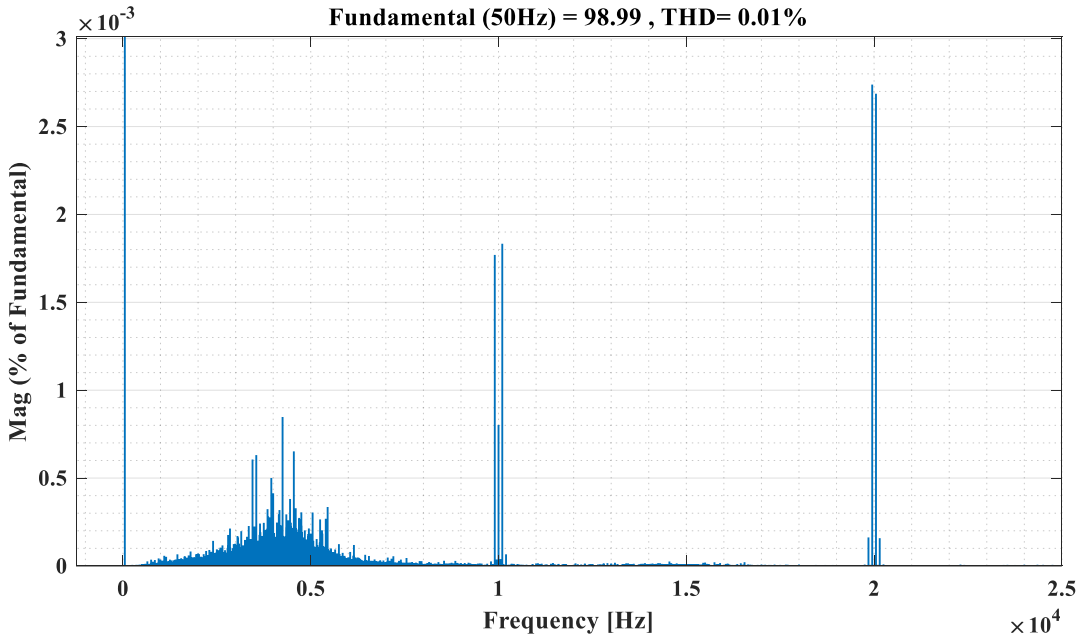

Figure 3.10: FFT analysis of inverter output voltage after filtering.

In Figures 3.9 and 3.10, the voltage waveform is sinusoidal, and the fundamental makeup 98.99% of the signal is due to the suppression of the harmonics at 10kHz and 20kHz.

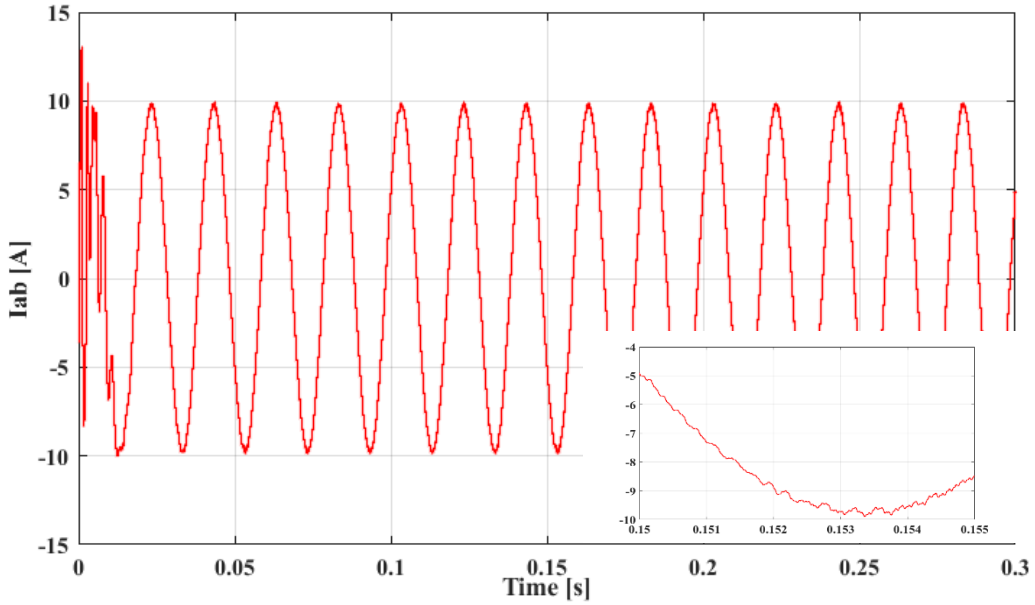

Figure 3.11: Filtered output current waveform of the inverter.

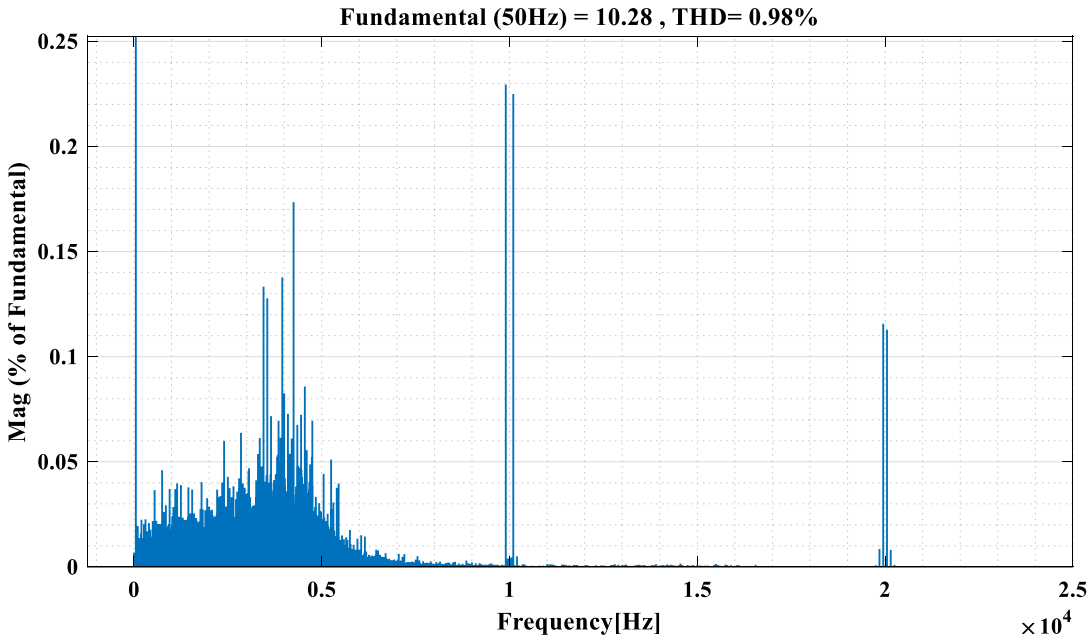

Figure 3.12: FFT analysis of inverter output current after filter

The application of an LCL filter at the output of the inverter in a three-phase grid-connected solar system led to a significant improvement in power quality. Before filtering, the system exhibited a total harmonic distortion (THD) of 124.83% for voltage and 2.76% for current, indicating severe harmonic issues. After filtering, these values significantly decreased

to 0.01% for voltage and 0.98% for current, demonstrating the effectiveness of the LCL filter in reducing harmonics and ensuring compliance with grid standards.

3.5 Three-Phase Voltage and Current Waveforms

In this simulation of three-phase voltage and current waveforms, you would observe three sinusoidal waveforms for both voltage and current, each phase shifted by 120 degrees, indicating a balanced system. The following results present the voltage and current waveforms, first employing a PI controller and then a PR controller in the inner current loop.

3.5.1 The Voltage and Current waveforms using the PI controller

Figures 3.13 and 3.14 show the waveforms for the three-phase grid voltage and current using a PI controller. Both waveforms are sinusoidal with minimal harmonic distortion. The voltage amplitude is 70 $[Vrms]$ line-to-line, while the current amplitude is 10.53 $[A]$. In this section, we implemented PI controller for the inner current loop of a three-phase grid-connected inverter solar system, aiming to regulate the I_d and I_q currents, thereby controlling the Iabc current. By applying the Particle Swarm Optimization (PSO) algorithm to obtain the PI parameters, we achieved the following results,

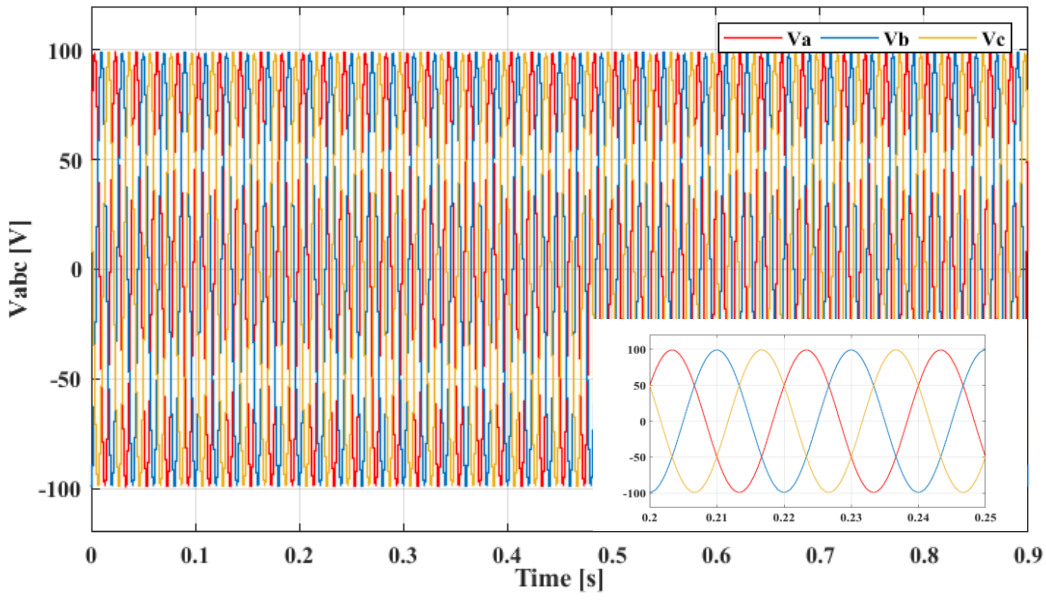

Fig 3.13: Output waveform of three-phase voltage for inverter using PI controller

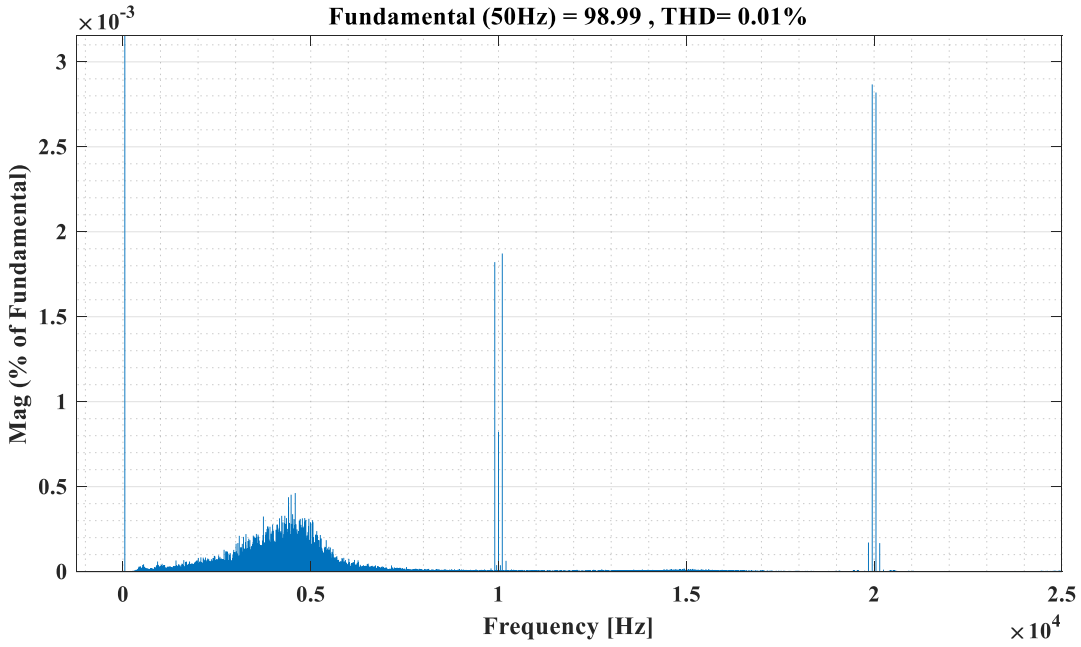

Figure 3.14: FFT analysis of inverter voltage

The system achieved a total harmonic distortion (THD) of 0.01% for voltage, as shown in Figure 3.14, and 1.13% for current, as shown in Figure 3.16, The magnitude of the fundamental components indicating a strong sinusoidal waveform with minimal distortion. The results reflect that the PI controller is still effectively controlling the three-phase inverter, producing a relatively clean sinusoidal current output with minimal harmonic distortion.

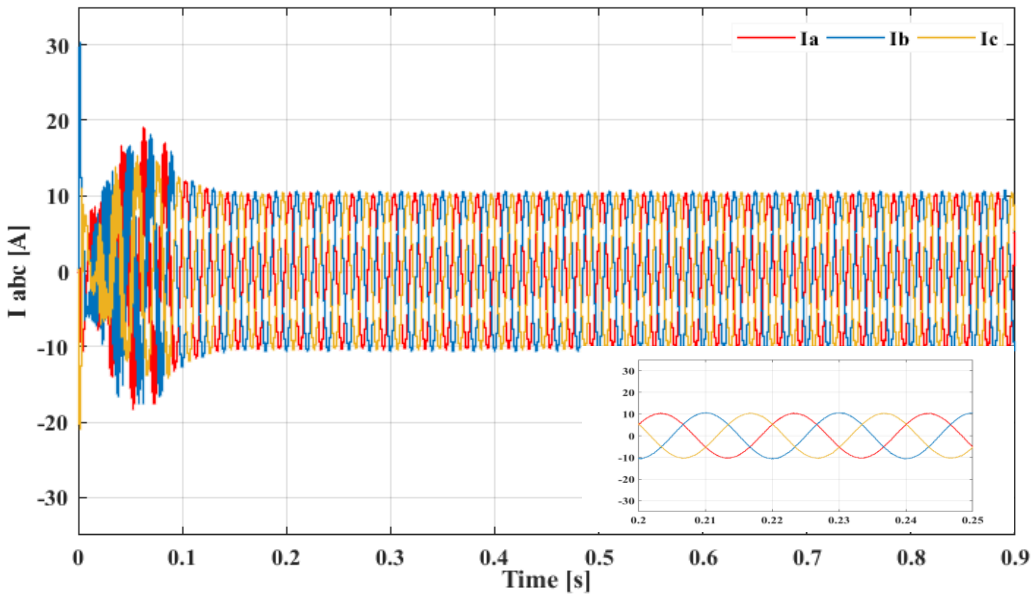

Figure 3.15: Output waveform of three-phase current for inverter using PI controller.

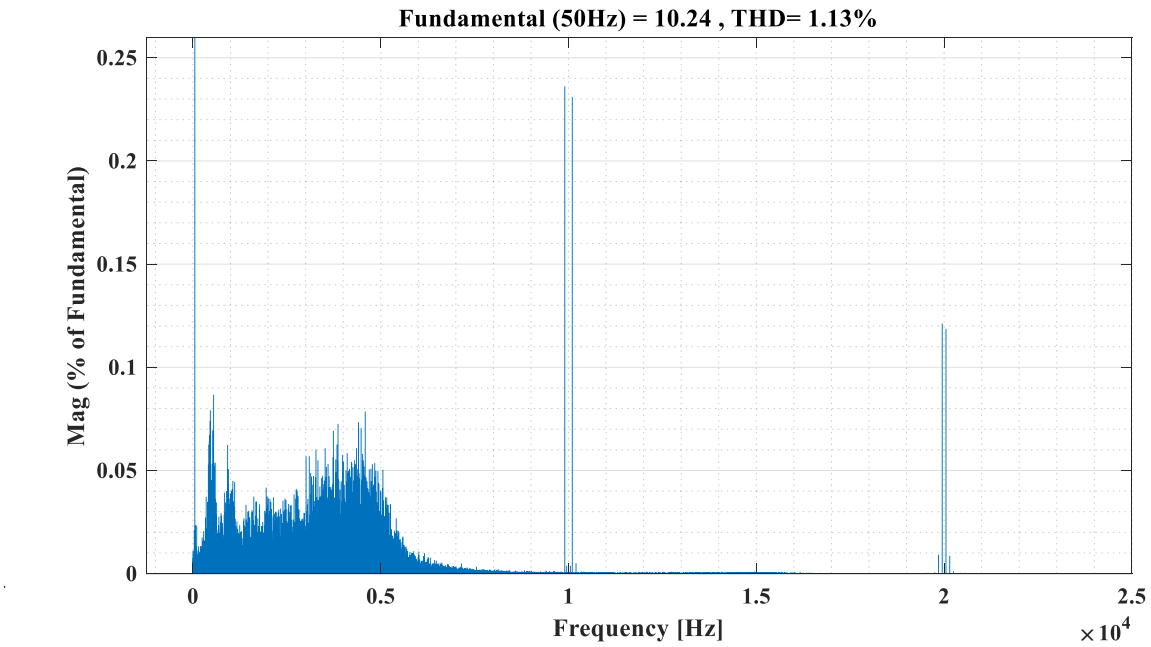

Figure 3.16: FFT analysis of inverter current

In Figure 3.17, the current loop controller is validated, showing that the measured I_d and I_q signals closely follow their respective reference values. This figure also highlights the fast response of the current controller, as it quickly reaches the desired references in a brief period. The I_d current, responsible for active power, while the I_q current, which controls reactive power, is maintained at zero.

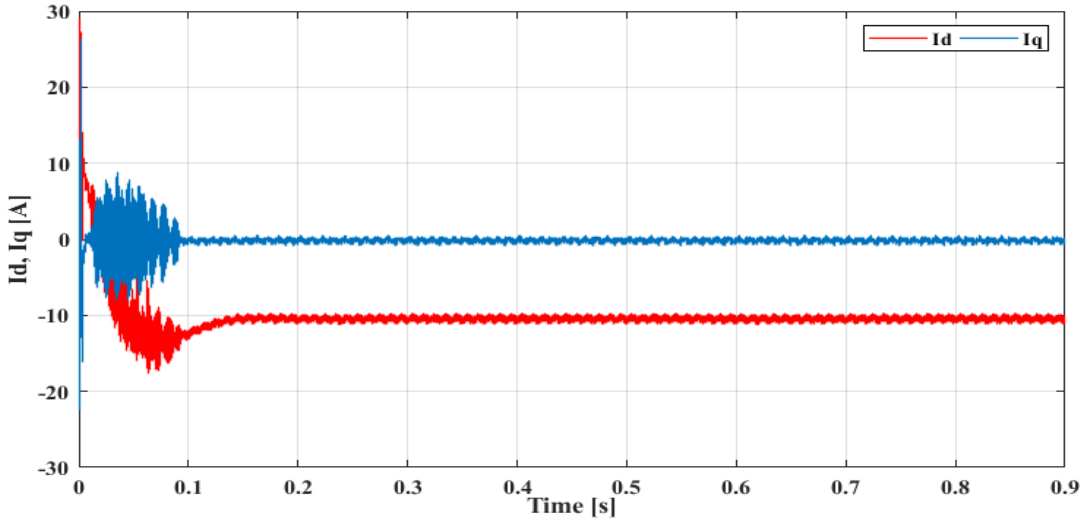

Figure 3.17: Direct and quadrature current component

In Figures 3.18 and Figures 3.19, the grid currents are shown increasing in relation to changes in I_d current under different assumed irradiance scenarios [$1000\,W/m^2$ $500\,W/m^2$ $300\,W/m^2$].

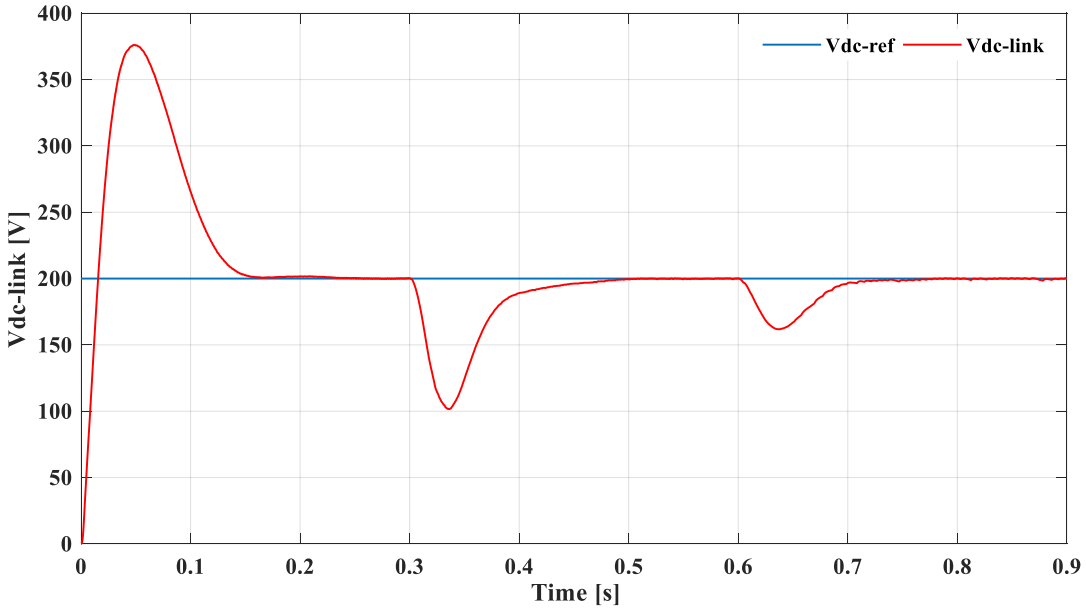

Figure 3.18: Vdc-link under different assumed irradiance scenarios in PI loop

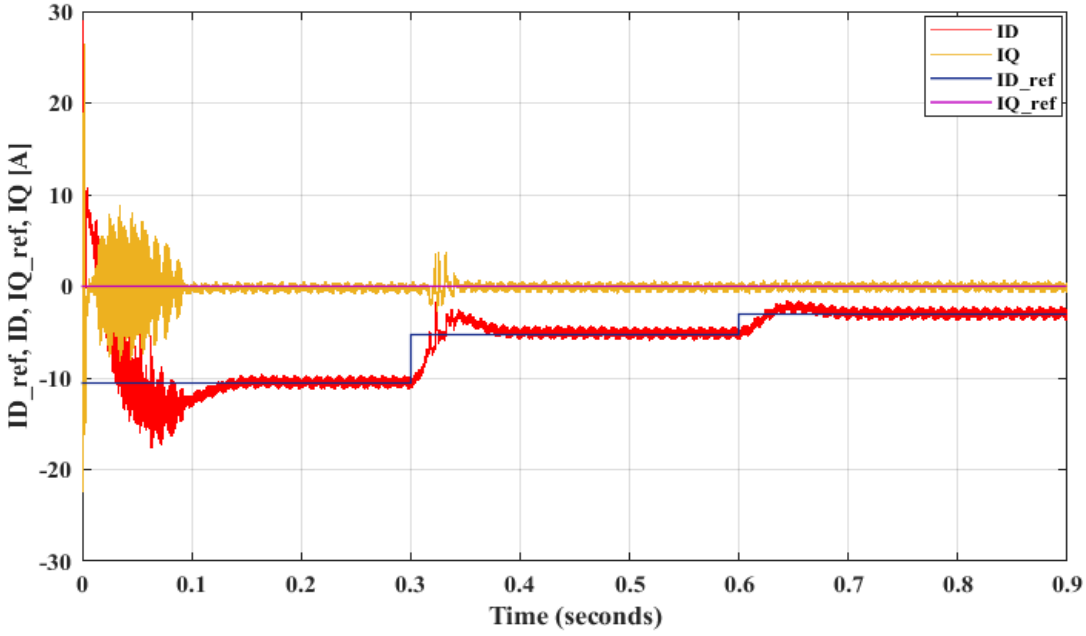

Figure 3.19: Direct current component under different assumed irradiance scenarios.

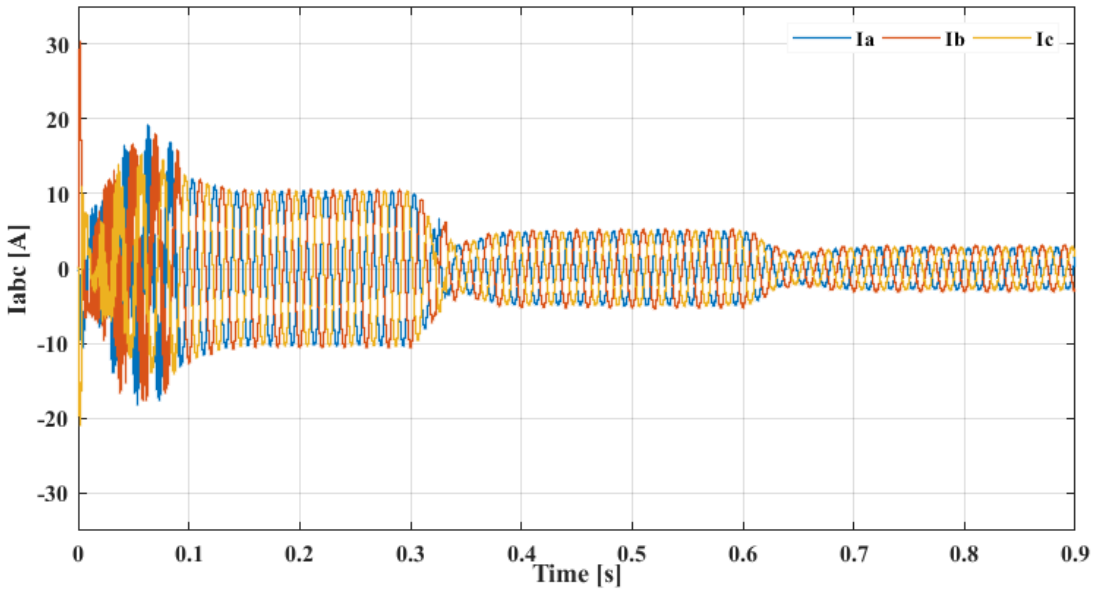

Figure 3.20: Output waveform of three-phase voltage for inverter under different assumed irradiance scenarios

The current varies in accordance with the irradiation level, demonstrating the effective performance of the PI controller in the inner current loop. The distortion observed in the current waveform at the initial moment and whenever the irradiation changes results from the settling time.

Table 3.2 provides the values for the PI controller parameters using POS algorithm.

Table 3.2: Parameters of PI controller for the inner current loop

Parameters	Values
K_p	54
K_i	5442

3.5.2 The Voltage and Current waveforms using PR controller

Figures 3.21 and 3.23 illustrate the waveforms for the three-phase grid voltage and current controlled by the PR controller. Both waveforms are sinusoidal and exhibit minimal harmonic distortion. The voltage and current amplitude are the same as mentioned before.

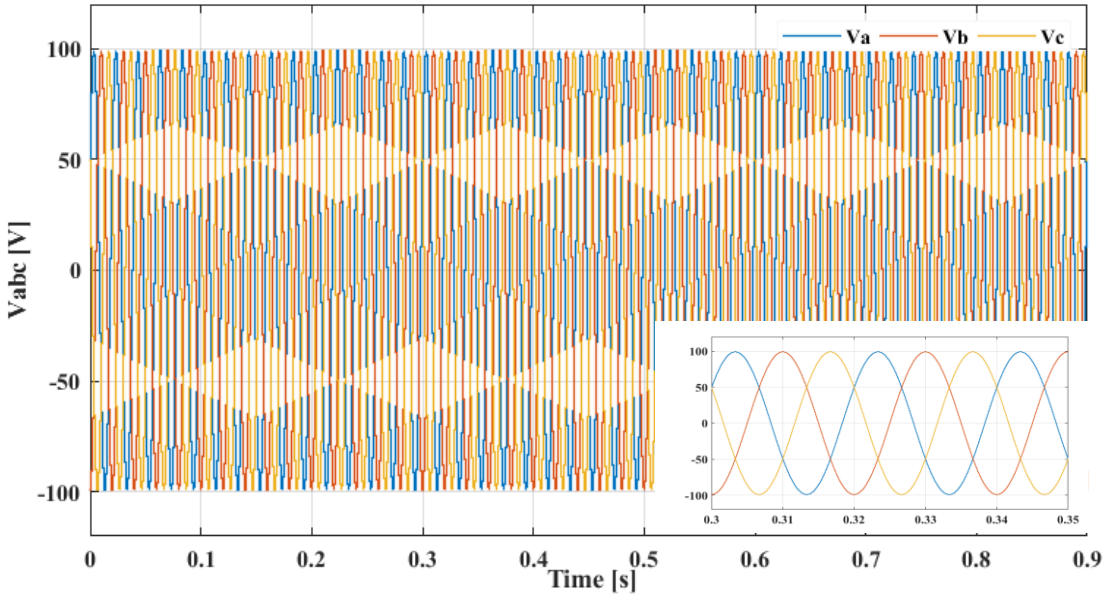

Figure 3.21: Output waveform of three-phase voltage for inverter using PR controller

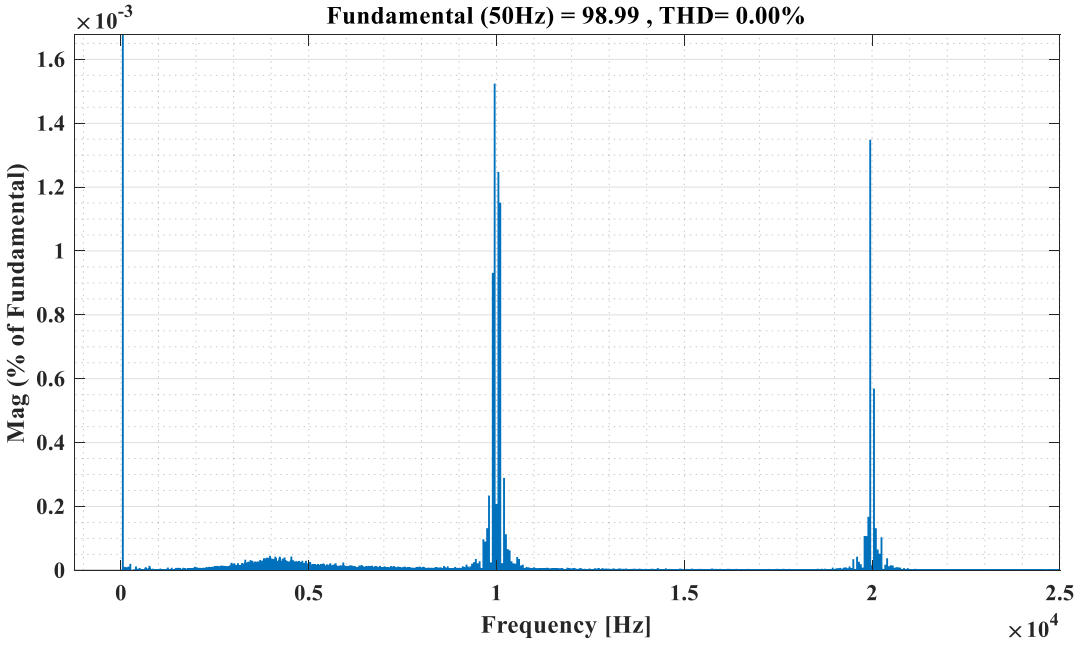

Figure 3.22: FFT analysis of inverter voltage

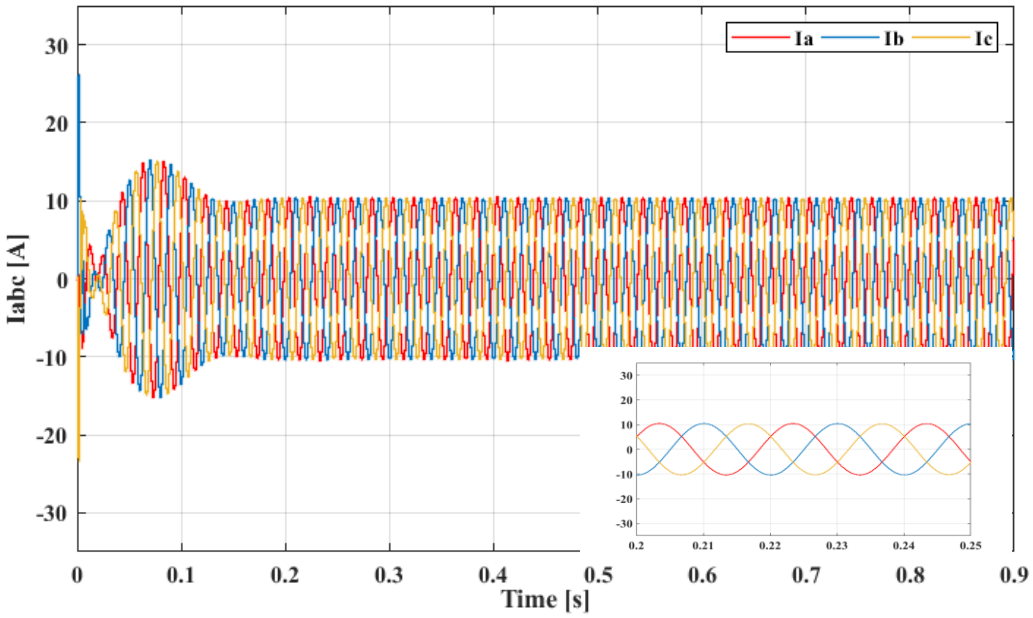

Figure 3.23: Output waveform of three-phase current for inverter using PR controller.

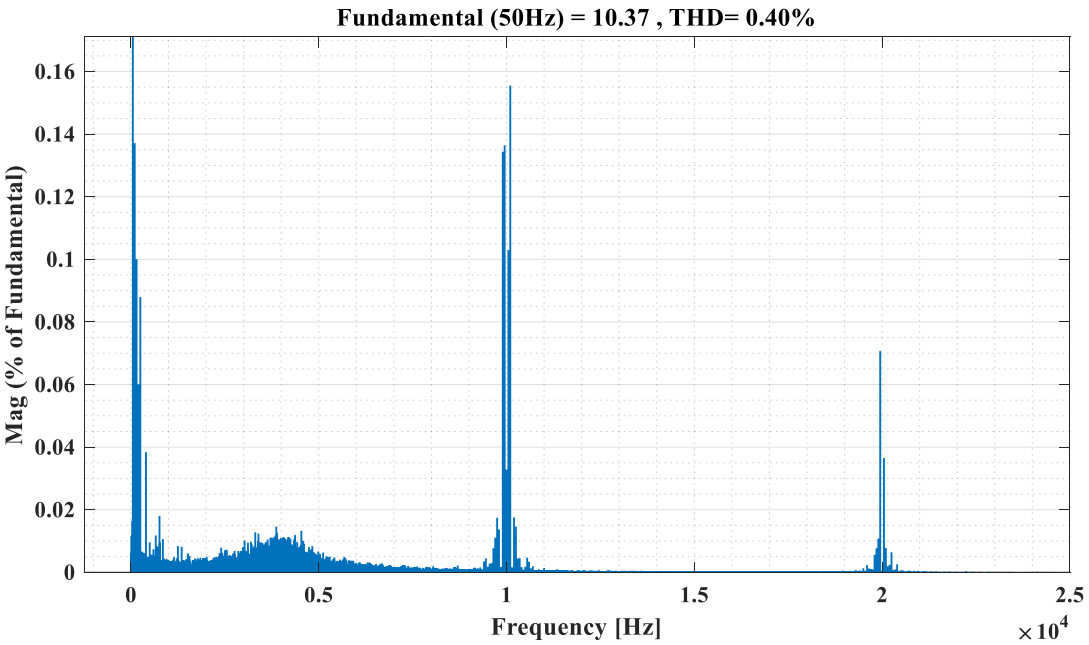

Figure 3.24: FFT analysis of inverter current

In this part, we applied a Proportional-Resonant (PR) controller to the inner and outer control loops of a three-phase grid-connected inverter solar system. The system achieved an exceptional total harmonic distortion (THD) of 0.00% for voltage, as Figure 3.22 illustrated, and 0.4% for current, as shown in Figure 3.24, The magnitude of the fundamental component is 10.37, indicating a strong sinusoidal waveform with minimal distortion, indicating excellent

performance in maintaining power quality. also; The THD is significantly lower than the previous result obtained with PI control. This suggests a significant improvement in harmonic content reduction using PR control.

The PR controller is applied in the stationary reference frame (αβ-frame) to minimize tracking errors for sinusoidal signals. The resonance component ensures that the PR controller provides high gain at the fundamental frequency, enabling effective management of sinusoidal currents.

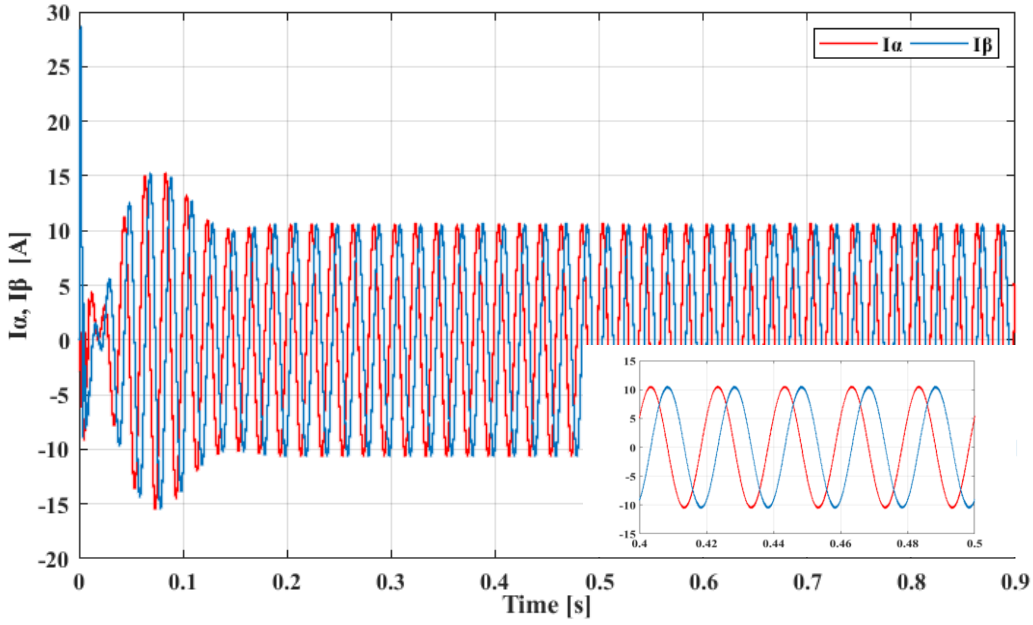

Figure 3.25: Alpha and beta current component

The simulation results shown in Figure 3.24 demonstrated effective control of the I_α and I_β currents using the PR controller in Simulink. The controller successfully minimized tracking errors, keeping the currents close to their desired sinusoidal shapes. The system exhibited strong dynamic performance with quick settling times and minimal overshoot, indicating its ability to handle fluctuations in reference signals. Additionally, the high gain at the fundamental frequency allowed for precise regulation of the sinusoidal currents, ensuring stable operation under varying load conditions. Overall, the results confirm the PR controller's effectiveness for the grid-connected inverter system.

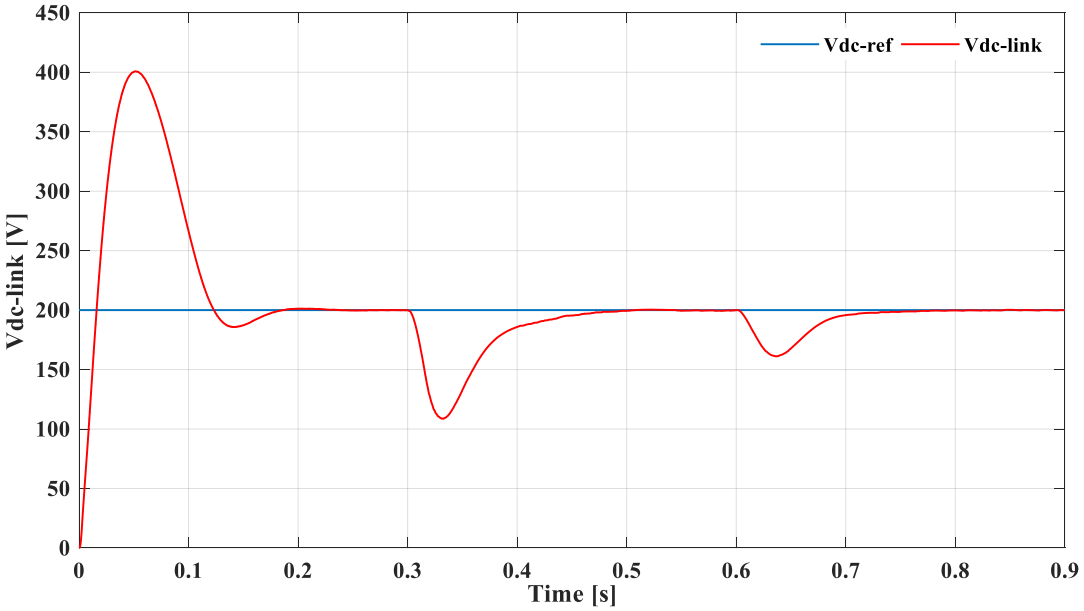

Figure 3.26: Vdc-link under different assumed irradiance scenarios in PR loop

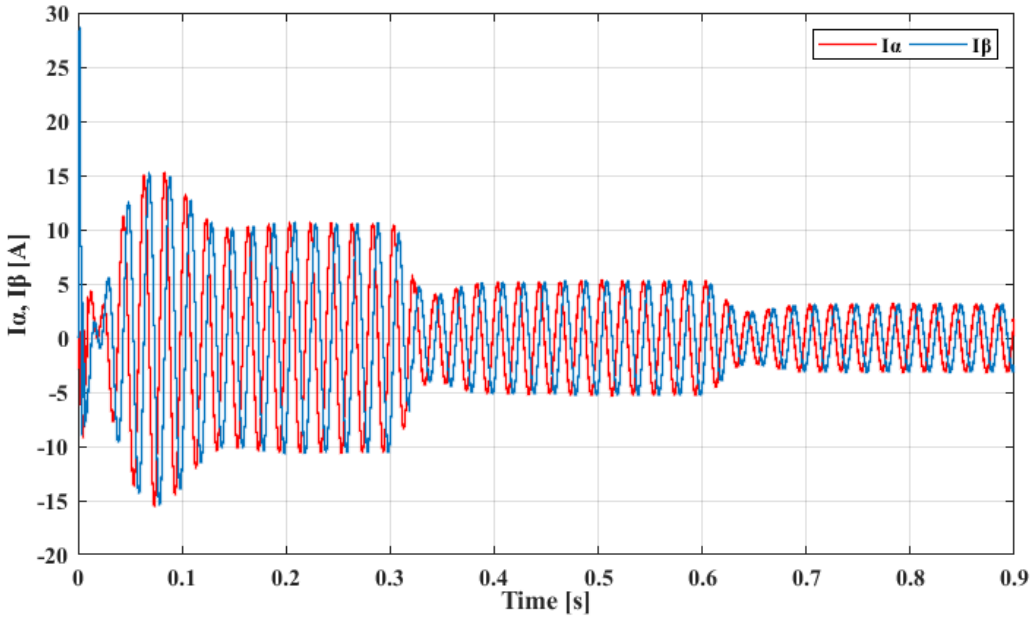

Figure 3.27: Alpha (α) and beta (β) components under different assumed irradiance scenarios

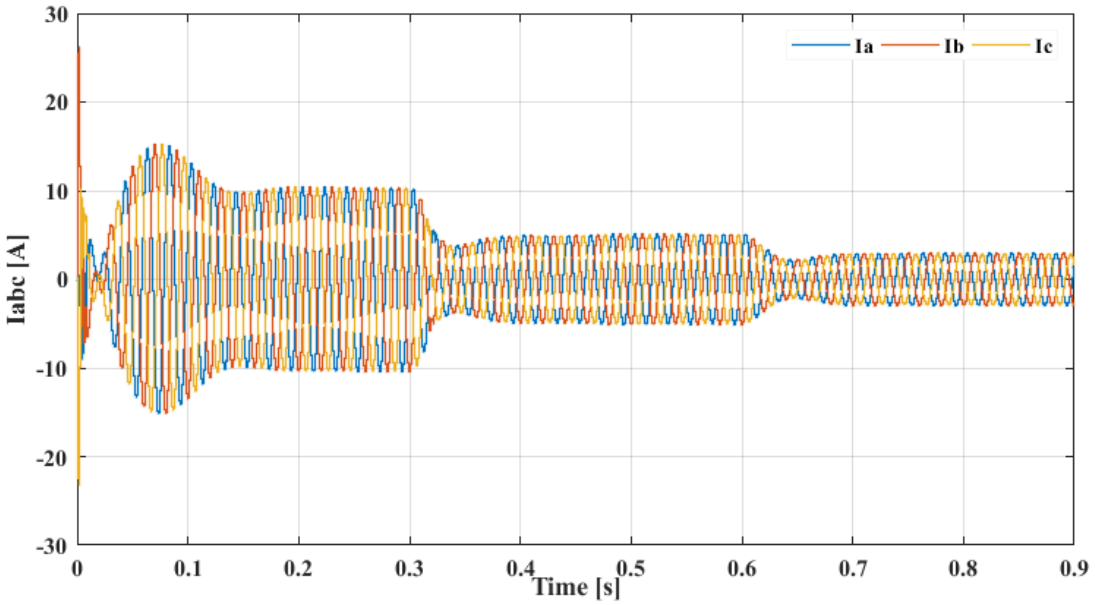

Figure 3.28: Output waveform of three-phase voltage for inverter under different assumed irradiance scenarios

In Figure 3.27 and 3.28, the grid currents are shown increasing in relation to the changes in I_α current under different assumed irradiance scenarios $[1000\,W/m^2 \quad 500\,W/m^2 \quad 300\,W/m^2]$, indicating the excellent performance of the PR controller in the inner current loop. The initial distortion in the current waveform, as well as that occurring with each change in irradiation, is caused by the settling time in the outer loop voltage.

Table 3.3 provides the values for the PR controller parameters using PSO algorithm.

Table 3.3: Parameters of PR controller for the inner current loop

Parameter	value
K_p	294.68
K_r	694.77

The results confirmed that PR control outperformed proportional-integral PI control in the three-phase grid-connected inverter solar system simulation. The PR controller demonstrated superior efficiency and required fewer steps in the control topology.

3.6 Implementation

The complete system is modeled and simulated with MATLAB Simulink, which offers an intuitive platform for designing and testing control strategies. This allows for real-time visualization of system performance. To enhance the performance and reliability of the control loops, the control algorithms are converted into hardware description language (HDL), specifically VHDL. This can be done in the following steps:

- Create a comprehensive Simulink model that accurately represents the desired functionality of the control algorithms. Ensure that all components are correctly configured and connected.
- Utilize blocks that are compatible with HDL code generation. Avoid using unsupported blocks such as certain MATLAB Function blocks and specific Simscape blocks.
- Implement the Data Type Conversion block to change any floating-point data to fixed-point formats where necessary.
- Launch the HDL Coder by typing *hdlcoder* in MATLAB or navigating through the Apps tab.
- In the HDL Coder interface, select the prepared Simulink model for HDL code generation.
- Open the "Configuration Parameters" dialog in HDL Coder and set the following: Choose VHDL as the target language and specify the target FPGA device or family.
- Click the “Generate HDL” button to create VHDL files from the Simulink model. Specify the output directory for the generated code files.

The generated HDL codes for different blocks are available in Appendix B.

3.7 Conclusion

This chapter detailed the simulation results of the DC-DC boost converter with an MPPT controller and inverter performance. The outer loop voltage THD was 0.92%, while the PI controller yielded a current THD of 1.13% and a voltage THD of 0.01%. Using a PR controller improved performance, achieving a current THD of 0.4% and a voltage THD of 0.00%. These results indicate that the PR controller is effectively controlling the three-phase inverter, producing a high-quality sinusoidal current output with minimal harmonic distortion. The improved performance compared to PI control highlights the benefits of using PR for this application.

General Conclusion

In this project, the design and modeling of a three-phase grid-connected solar PV system using a stationary reference frame and synchronously rotating reference frame have been successfully achieved. The proposed system includes a PV array, a DC-DC boost converter, an Incremental Conductance-based Maximum Power Point Tracking (MPPT) method, a three-phase Voltage Source Inverter (VSI), and an LCL filter. The DC-DC boost converter was designed to boost the output voltage of the PV array to the required level. Control algorithms were proposed to maximize the output power from the PV array. Key components of the system include the Maximum Power Point Tracking (MPPT), DC-link regulator, active and reactive power control, total harmonic elimination, and synchronization control. Simulation results demonstrate that the Perturb and Observe-based MPPT method successfully identifies the maximum power point of the PV array, enabling it to extract the highest possible power based on the current environmental conditions. A three-phase voltage source inverter was controlled using stationary SR and SRRF with SVPWM to convert the DC voltage to an AC voltage in which its output current is synchronized with the grid voltage. An LCL filter was designed to reduce and attenuate the high-frequency harmonics at the output side of the inverter. This filter is used to interconnect the inverter output with the grid, which provides the filtering of harmonics available in the current due to the switching nature of the inverter. The inverter's control structure consists of two loops: an external loop for managing DC-link voltage and an internal loop for current control. These loops work together to regulate power flow within the system and ensure power quality by addressing harmonics in the current. The simulation results show that the proposed system operates efficiently and effectively under various weather conditions. The total harmonic distortion of the grid current and voltage using the SRRF technique with a PI controller is 1.13% and 0.01%, respectively, whereas the stationary SR with a PR controller achieves 0.4% and 0.0%, showing that the latter is more effective.

Future Work

The following is a list of recommendations for future project developments:

- Deploy the VHDL codes we generated from HDL in a hardware-in-the-loop setup.
- Perform some practical experiments to verify the obtained simulation results.
- It is possible to compare the model developed based on perturb and observe to different types of MPPT techniques.
- Perform fault analysis on the developed system model using the constructed model.

[1] Tomas Markvart (2001, „“Solar Electricity““, John wiley& sons Baffin“s Lane chichester west Sussex P019IUD, England,p-25.

[2] Green et al., “Solar cell efficiency tables (version 49),” Progress in Photovoltaics: Research and Applications, vol. 25, no. 1. pp. 3–13, Jan. 2017.

[3] S. Sumathi, L. Ashok Kumar, and P. Surekha, „“Solar PV and Wind Energy Conversion Sytems’’.

[4] M. A. Elgendy, B. Zahawi and D. J. Atkinson, "Evaluation of perturb and observe MPPT algorithm implementation techniques," 6th IET International Conference on Power Electronics, Machines and Drives (PEMD 2012), Bristol, pp. 1-6, 2012.

[5] M. G. G. Villalva et al., “Comprehensive Approach to Modeling and Simulation of Photovoltaic Arrays,” IEEE Transactions on Power Electronics, vol. 24, no. 5. pp. 1198–1208, May 2009.

[6] Rashid, Power Electronics: Circuits, Devices, and Applications, 3rd ed. Prentice Hall, 2003.

[7] Mohan et al., Power Electronics: Converters, Applications and Design, 3rd ed. John Wiley& Sons, Ltd, 2003.

[8] J. Jana, H. Saha and Das Bhattacharya, "A review of inverter topologies for single-phase grid-connected photovoltaic systems", Renewable and Sustainable Energy Reviews, vol. 72, pp. 1256-1270, 2017.

[9] F. Blaabjerg et al., “Overview of Control and Grid Synchronizations of DPG Systems,” IEEE Transactions on Industrial Electronics, vol.53, no. 5. pp. 1398–1409, 2006.

[10] Digital Signal Processing Based Electromechanical Motion Control, 2004.

[11] L. N. Arruda, S. M. Silva “Phase Locked Loop structures for utility Grid connected systems,” in Proc. IEEE-IAS Annu. Meeting, vol. 4, pp. 2655–2660, 2002.

[12] S. Kjaer, J. Pedersen and Blaabjerg, "A Review of Single-Phase Grid-Connected Inverters for Solar Photovoltaic Systems", IEEE Transactions on Industry Applications, vol. 41, no. 5, pp. 1292-1306, 2005.

[13] IEC 61727. Solar Photovoltaic systems – characteristics of the utility interface 2004.

[14] IEEE 1547. Standards for Interconnecting DRs with Electric Power Systems, 2003.

[15] IEEE Standard 929. IEEE Recommended Practice for Utility Interface of solar PV Systems, 2000.

[16] M. Prodanovic and T. Green, "Control and filter design of three-phase inverters for high power quality grid connection," in IEEE Transactions on Power Electronics, vol. 18, no. 1, pp. 373 380, 2003.

[17] Mohan, N., Undeland, T. M., & Robbins, W. P. (2003). *Power Electronics: Converters, Applications, and Design* (3rd ed.). Wiley.

[18] IEEE Standard 1547-2018. (2018). *IEEE Standard for Interconnection and Interoperability of Distributed Energy Resources with Associated Electric Power Systems Interfaces*.

[19] Rezvani, A., Tavakoli, S. M. M., & Abolfazli, M. S. (2020). Grid-connected photovoltaic inverters: A review on issues, challenges, and options. *Renewable and Sustainable Energy Reviews*, 120, 109646.

[20] M. Rashid, Power electronics handbook, 3rd ed. Elsevier, 2011.

[21] G. M. Masters, Renewable and Efficient Electric Power Systems. Hoboken, NJ, USA: John Wiley & Sons, Inc., 2004.

[22] R. Kadri, J. P. Gaubert, and G. Champenois, "An Improved Maximum Power Point Tracking for Photovoltaic Grid-Connected Inverter Based on Voltage-Oriented Control," IEEE Trans, Ind. Electronic., vol. 58, pp. 66-75, 2011.

[23] M. A. Elgendy, B. Zahawi, and D. J. Atkinson, "Operating Characteristics of the P&O Algorithm at High Perturbation Frequencies for Standalone PV Systems," IEEE Transactions on Energy Conversion, vol. 30, pp. 189-198, 2015.

[24] Liu X, Wang P & Loh PC (2010), „"Optimal Coordination Control for Standalone PV System with Nonlinear Load"", Proceedings of 2010 9th international power and energy conference, Singapore, 27-29October 2010, 5pp.

[25] Grandi G, Rossi C, Ostojic D et al (2009) A new multilevel conversion structure for grid connected PV applications. IEEE Trans Ind Electron 56(11):4416–4426.

[26] Mohan N, Under land TM (2007) Power electronics: converters, applications, and design. Wiley, New York.

[27] F. Gao, D. Li, P. C. Loh, Yi Tang and Peng Wang, "Indirect dc-link voltage control of two stage single-phase PV inverter," 2009 IEEE Energy Conversion Congress and Exposition, San Jose, CA, pp. 1166-1172, 2009.

[28] L. N. Arruda, S. M. Silva "Phase Locked Loop structures for utility Grid connected systems," in Proc. IEEE-IAS Annu. Meeting, vol. 4, pp. 2655–2660, 2002.

[29] Koutroulis, E., Potirtis, A., & Kalogirou, S. A. (2001). "Development of a microcontroller-based, photovoltaic maximum power point tracking control system." *IEEE Transactions on Power Electronics*, 16(1), 46-54.

[30] K. Zhou and Wang, “Relationship between space-vector modulation and three-phase carrier-based PWM: a comprehensive analysis [three-phase inverters],” IEEE Transactions on Industrial Electronics, vol. 49, no. 1. pp. 186–196, 2002.

[31] W.F.Zhang et al., “Comparison of Three SVPWM Strategies,” Journal of Electronic Science and Technology, vol. 5, no. 3. Editorial Board of Journal of University of Electronic Science and Technology, pp. 283–287, 2007.

[32] M.-Y.Park et al., “an LCL filter design for grid-connected PCS using THD and RAF,” The 2010 International Power Electronics Conference - ECCE ASIA -. IEEE, pp. 1688–1694, Jun. 2010.

[33] X. Wei et al., “Design of LCL filter for wind power inverter,” in 2010 World NonGridConnected Wind Power and Energy Conference, 2010, pp. 1-6.

[34] T. C. T. C. Y. Wang et al., “Output filter design for a grid-interconnected three-phase inverter,” in IEEE 34th Annual Conference on Power Electronics Specialist, 2003, vol. 2, pp. 779–784.

[35] Lissere. M. et al., “Design and control of an LCL filter based three-phase active rectifier,” IEEE Transactions on Industry Applications, vol. 41, no. 5. pp. 1281– 1291, Sep. 2005.

[36] H. Cha and Vu, “Comparative analysis of low-pass output filter for single-phase grid-connected Photovoltaic inverter,” in Twenty-Fifth Annual IEEE Applied Power Electronics Conference and Exposition (APEC), 2010 pp. 1659–1665.

[37] WorkagegnTatek, “Model reference adaptive control based sensorless speed control of induction motor”, 2017.

[38] Suresh Lakhimsetty, “Simulation of space vector PWM for voltage source inverter using matlab/Simulink““, 2014.

[39] D. Candusso, L. Valero, A. Walter, S. Bacha, E. Rulliere and B. Raison, "Modeling, control and simulation of a fuel cell based on power supply system with energy management," IEEE 2002 28th Annual Conference of the Industrial Electronics Society. IECON 02, pp. 1294-1299 vol.2, 2002.

[40] C. Ramos, A. Martins, and Carvalho, “Current control in the grid connection of the double output induction generator linked to a variable speed wind turbine,” in Proc. IEEE IECON, vol.2, pp. 979–984, 2002.

[41] M. Bhardwaj, “Software phased-locked loop design using c2000TM micro-controllers for three phase grid connected applications,” tech. rep., Texas Instruments, 2013.

[42] D’Apice, C., Manzo, R., & Nasti, E. (2020). Control techniques for grid-connected inverters: A comparative analysis of PI and PR regulators. *International Journal of Power Electronics and Drive Systems*, 11(1), 89-99.

[43] H. K. S. Gupta, P. T. Krein, and C. H. Wu, "Voltage Control in DC-Link for Grid-Connected Inverter Systems", IEEE Transactions on Power Electronics, vol. 32, no. 5, pp. 3874-3884, May 2017.

[44] S. Fahad, A. J. Mahdi, W. H. Tang, K. Huang, and Y. Liu**,** "Particle Swarm Optimization Based DC-Link Voltage Control for Two Stage Grid Connected PV Inverter," *Energy Reports*, vol. 4, pp. 2233-2241, 2018.

[45] L. Ma, W. Ran and T. Q. Zheng, "Modeling and control of three phase grid-connected photovoltaic inverter," Control and Automation (ICCA), 2010 8th IEEE International Conference on, Xiamen, 2010, pp. 2240-2245.

[46] Adrian Timbus, Marco Liserre, Remus Teodorescu, Pedro Rodriguez, and Frede Blaabjerg," Evaluation of Current Controllers for Distributed Power Generation Systems", IEEE TRANSACTIONS ON POWER ELECTRONICS, VOL. 24, NO. 3, MARCH 2009.

[47] Remus Teodorescu, and Frede Blaabjerg," Flexible Control of Small Wind Turbines With Grid Failure Detection Operating in Stand-Alone and Grid-Connected Mode", IEEE TRANSACTIONS ON POWER ELECTRONICS, VOL. 19, NO. 5, SEPTEMBER 2004.

[48] Adrian Timbus, Marco Liserre, Remus Teodorescu, Senior Member, Pedro Rodriguez, and Frede Blaabjerg," Evaluation of Current Controllers for Distributed Power Generation Systems", IEEE TRANSACTIONS ON POWER ELECTRONICS, VOL. 24, NO. 3, MARCH 2009.

[49] J.Kennedy and R. Eberhart, "Particle swarm optimization," in Neural Networks, 1995. Proceedings., IEEE International Conference on, 1995, pp. 1942-1948 vol.4.

Appendices

appendix A

```
VLLrms = 70; % line to line rms voltage
Vph = 70/sqrt(3); % phase rms voltage
Pn = 800; % rated active power (Pmpp at STC)
Vdc = 200; % dc-link voltage from the boost converter
fg = 50; % grid frequency
fs = 10e3; % inverter switching frequency
%Step1-----Calculate Zb,Lb,Cb
Vb=VLLrms;
Pb=Pn;
Ib=Pn/(sqrt(3)*VLLrms);
Zb=VLLrms^2/Pn;
Lb=Zb/(2*pi*fg);
Cb=1/(2*pi*fg*Zb);
%Step2-----Calculate Cf (maximum power factor variation seen by the grid is less than 5%)
x=2.5/100;
Cf=x*Cb
%Step3-----Calculate Li (deltaIb=Vdc/(8*fs*Li)) deltaIb between 10-20%
deltaIb=0.2*Ib; %(20% * Imax)
Li=Vdc/(8*fs*deltaIb)
%Step4-----Calculate Lg
RAF = 20/100; % attenuation factor is 20%
Lg=(RAF+1)/(RAF*Cf*(2*pi*fs)^2)
%Step5-----Calculate frequency resonance
Ur=sqrt((Li+Lg)/(Li*Lg*Cf));
fres=Ur/(2*pi); % resonance frequency
%Step6-----make sure that 10fg<(fres)<fs/2
fres_Test=(fres>10*fg) && (fres<fs/2);
%Step7-----Calculate damping resistor( Rf)
```

Rf=1/(3*2*pi*fres*Cf)

Appendix B

mppt HDL

```
-- -------------------------------------------------------------
--
-- File Name: hdlsrc\mpptHDL\mpptHDL.vhd
-- Created: 2024-09-24 08:29:22
--
-- Generated by MATLAB 9.4 and HDL Coder 3.12
--
--
-- -------------------------------------------------------------
-- Rate and Clocking Details
-- -------------------------------------------------------------
-- Model base rate: 0.0001
-- Target subsystem base rate: 0.0001
--
--
-- Clock Enable  Sample Time
-- -------------------------------------------------------------
-- ce_out        0.0001
-- -------------------------------------------------------------
--
--
-- Output Signal                 Clock Enable  Sample Time
-- -------------------------------------------------------------
-- duty_cycle                    ce_out        0.0001
-- -------------------------------------------------------------
--
-- -------------------------------------------------------------
```

```
-- -------------------------------------------------------------
--
-- Module: mpptHDL
-- Source Path: mpptHDL
-- Hierarchy Level: 0
--
-- -------------------------------------------------------------
LIBRARY IEEE;
USE IEEE.std_logic_1164.ALL;
USE IEEE.numeric_std.ALL;

ENTITY mpptHDL IS
  PORT( clk                         :   IN    std_logic;
        reset                       :   IN    std_logic;
        clk_enable                  :   IN    std_logic;
        V_pv                        :   IN    real;  -- single
        I_pv                        :   IN    real;  -- single
        ce_out                      :   OUT   std_logic;
        duty_cycle                  :   OUT   real  -- single
        );
END mpptHDL;


ARCHITECTURE rtl OF mpptHDL IS

  -- Signals
  SIGNAL enb                        : std_logic;
  SIGNAL P_out1                     : real := 0.0;  -- single
  SIGNAL Unit_Delay_out1            : real := 0.0;  -- single
  SIGNAL deltaP_out1                : real := 0.0;  -- single
  SIGNAL switch_compare_1           : std_logic;
  SIGNAL Unit_Delay1_out1           : real := 0.0;  -- single
```

```
  SIGNAL deltaV_out1                : real := 0.0;  -- single
  SIGNAL switch_compare_1_1         : std_logic;
  SIGNAL Gain_out1                  : real := 0.0;  -- single
  SIGNAL Constant3_out1             : real := 0.0;  -- single
  SIGNAL Switch1_out1               : real := 0.0;  -- single
  SIGNAL switch_compare_1_2         : std_logic;
  SIGNAL Switch_out1                : real := 0.0;  -- single
  SIGNAL Switch2_out1               : real := 0.0;  -- single
  SIGNAL Saturation_out1            : real := 0.0;  -- single
  SIGNAL Unit_Delay2_out1           : real := 0.0;  -- single
  SIGNAL Add2_out1                  : real := 0.0;  -- single

BEGIN
  P_out1 <= V_pv * I_pv;
  enb <= clk_enable;

  Unit_Delay_process : PROCESS (clk, reset)
  BEGIN
    IF reset = '1' THEN
      Unit_Delay_out1 <= 0.0;
    ELSIF clk'EVENT AND clk = '1' THEN
      IF enb = '1' THEN
        Unit_Delay_out1 <= P_out1;
      END IF;
    END IF;
  END PROCESS Unit_Delay_process;
   deltaP_out1 <= P_out1 - Unit_Delay_out1;
  switch_compare_1 <= '1' WHEN deltaP_out1 > 0.0 ELSE
      '0';
  Unit_Delay1_process : PROCESS (clk, reset)
  BEGIN
    IF reset = '1' THEN
```

```
    Unit_Delay1_out1 <= 0.0;
  ELSIF clk'EVENT AND clk = '1' THEN
    IF enb = '1' THEN
      Unit_Delay1_out1 <= V_pv;
    END IF;
  END IF;
END PROCESS Unit_Delay1_process;
deltaV_out1 <= V_pv - Unit_Delay1_out1;
switch_compare_1_1 <= '1' WHEN deltaV_out1 > 0.0 ELSE
    '0';
Gain_out1 <= (-0.0123);
Constant3_out1 <= 0.0123;
Switch1_out1 <= Gain_out1 WHEN switch_compare_1_1 = '0' ELSE
    Constant3_out1;
switch_compare_1_2 <= '1' WHEN deltaV_out1 > 0.0 ELSE
    '0';
Switch_out1 <= Constant3_out1 WHEN switch_compare_1_2 = '0' ELSE
    Gain_out1;
Switch2_out1 <= Switch1_out1 WHEN switch_compare_1 = '0' ELSE
    Switch_out1;

Unit_Delay2_process : PROCESS (clk, reset)
BEGIN
  IF reset = '1' THEN
    Unit_Delay2_out1 <= 0.0;
  ELSIF clk'EVENT AND clk = '1' THEN
    IF enb = '1' THEN
      Unit_Delay2_out1 <= Saturation_out1;
    END IF;
  END IF;
END PROCESS Unit_Delay2_process;
Add2_out1 <= Switch2_out1 + Unit_Delay2_out1;
```

```
  Saturation_out1 <= 1.0 WHEN Add2_out1 > 1.0 ELSE
     0.0 WHEN Add2_out1 < 0.0 ELSE
     Add2_out1;
  ce_out <= clk_enable;
  duty_cycle <= Saturation_out1;
END rtl;
```